INVERSE SCATTERING
BY CONDUCTING CIRCULAR CYLINDERS

by

Raymond Cunningham Murphy, S.B. (M.I.T.)

INVERSE SCATTERING

BY CONDUCTING CIRCULAR CYLINDERS

by

Raymond Cunningham Murphy, S.B. (M.I.T.)

Department of Electrical Engineering
Master of Engineering

ABSTRACT

The reconstruction of near-fields from far-field pattern data is studied using a Fourier analysis-Bessel function technique. It is found that the surface of a conducting cylinder may be accurately located for pattern function data good to 3-4 decimal places, but that translated systems involve some loss of accuracy due to induced asymmetry. The information content of the scattering system is studied, and shows particular relevance when the reconstruction utilizes sectors of the 360^{o} pattern function. Further, bounds are derived for the range of Fourier coefficients necessary for accurate reconstruction. Finally, excellent agreement is found between the reconstructed near field and available experimental data.

INVERSE SCATTERING
BY CONDUCTING CIRCULAR CYLINDERS

by

Raymond Cunningham Murphy, S.B. (M.I.T.)

A thesis submitted to the Faculty of Graduate Studies
and Research in partial fulfillment of the
requirements for the degree of
Master of Engineering

Department of Electrical Engineering,
McGill University,
Montreal, Quebec,
July, 1971.

ABSTRACT

The reconstruction of near-fields from far-field pattern data is studied using a Fourier analysis-Bessel function technique. It is found that the surface of a conducting cylinder may be accurately located for pattern function data good to 3-4 decimal places, but that translated systems involve some loss of accuracy due to induced asymmetry. The information content of the scattering system is studied, and shows particular relevance when the reconstruction utilizes sectors of the 360^{o} pattern function. Further, bounds are derived for the range of Fourier coefficients necessary for accurate reconstruction. Finally, excellent agreement is found between the reconstructed near field and available experimental data.

ACKNOWLEDGEMENT

I would like to express my gratitude to Dr. T.J.F. Pavlasek, my research advisor, for his help in matters ranging from simple but frustrating administrative details to invaluable suggestions concerning the form of the entire study. Also, I would like to thank all the members of the Electromagnetics Research Group for their assistance and for many interesting discussions.

This project was supported by the National Research Council of Canada under grant A-515.

CONTENTS

INTRODUCTION

The subject of inverse scattering is concerned with the techniques used to relate scattering measurements to information about the scattering object. It includes such areas of interest as the determination of molecular, atomic, and nuclear structure; radar object identification; sonar location of sea life and submarines; geophysical and mineralogical research with patterned explosions; and antenna synthesis from a desired radiation pattern. The techniques include variations of scattering matrix inversion (Faddeyev and Seckler (1963); Boerner, Vandenberghe, and Hamid (1971)); reciprocal kernel method; Fourier transform of the scattering matrix (Weston and Boerner (1969)); and straightforeward electromagnetic techniques suitable for analytic continuation (Mittra (1970); Weston and Boerner (1969)). Also available for high-frequency limits is the geometrical approximation (Weiss (1968)).

In this thesis we will treat in detail the inverse scattering of cylindrical conductors using a Fourier analysis-Bessel function technique that can be included in the analytic continuation classification. We will be especially interested in the numerical aspects of the process. The study is conducted in such a way that the limitations of the techniques are emphasized. The first three chapters discuss the classical scattering problem for conducting cylinders, the relatively simple inverse scattering method, and the changes that make the scheme computable. Chapter 4 discusses some information and sampling concepts related to the problem, and

Chapter 5 chronologs a number of studies of near-field reconstruction from the far-field pattern function. Included are several graphs which will be useful for assuring accuracy in further reconstruction studies using this inverse scattering technique.

CHAPTER I

SCATTERING THEORY FOR CYLINDERS

Scattering of electromagnetic radiation by a conducting circular cylinder is one of the basic scattering problems, since there is an exact analytic solution in the cylindrical coordinate system coincident with the scattering cylinder. Kerker (1969) presents a concise treatment of scattering by homogeneous circular cylinders, and the special case of the conducting cylinder follows when the proper limits are applied to the equations describing the general solution.

For any boundary-value problem involving a wave-type solution, a complex wavefunction ψ may be defined over the region of interest, subject to the appropriate boundary constraints. For scattering problems we normally let the exterior boundary of the space be at infinity, and so a suitable boundary condition, known as the radiation condition, is imposed on all possible wave solutions. For a cylindrical geometry, this requires the magnitude of the scattered wave function to decrease at least as quickly as $1/\rho$. These solutions must satisfy the wave equation:

$$(\nabla^2 + k^2)\psi = 0 \qquad (1.1)$$

∇^2 is the Laplacian operator associated with the coordinate system. In this study we will restrict ourselves to the case of electric field parallel to the cylinder axis, which eliminates polarization effects and enables us to treat the superposition of

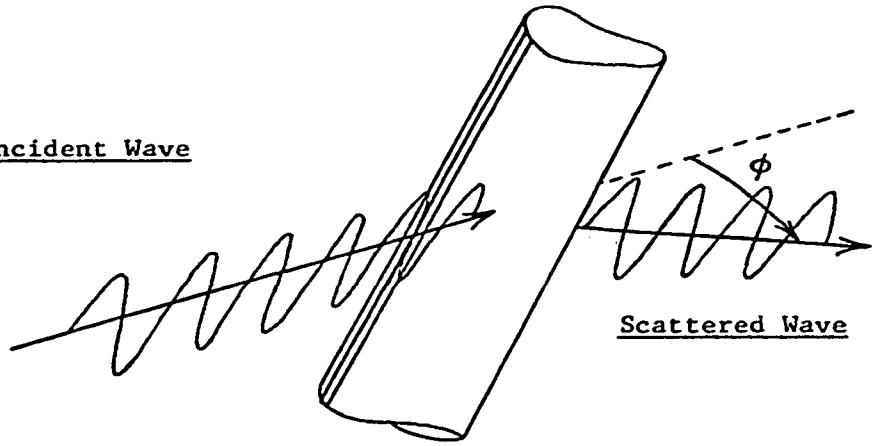

Figure 1.1 : Pictoral representation of the scattering process, showing an incident plane wave together with a wave scattered at an angle ϕ from the incident direction. The waves are axially polarized.

incident and scattered waves in a scalar manner. For our case of a conducting cylinder, the solution is also subject to the boundary condition $\psi=0$ on all conducting surfaces.

Our experiment will be conducted using a plane wave as the incident test function. Therefore we can proceed readily with an analysis in terms of Bessel functions. For an incident plane wave E-polarized along the cylinder axis, we choose a propagation direction x, and let

$$\psi_{inc} = E_z^i = E_0 e^{-jkx} = E_0 e^{-jk\rho\cos\phi} = E_0 \sum_{m=-\infty}^{\infty} j^{-m} J_m(k\rho) e^{jm\phi} \qquad (1.2)$$

The last step shown is the definition of the expansion in terms of a Fourier-Bessel series (Harrington (1961)). The total field at

any point outside the cylinder is the sum of contributions due to the incident and scattered waves:

$$E_z = E_z^i + E_z^s \tag{1.3}$$

and the requirements imposed by the physics of the experiment (scattered waves propagating away from the cylinder, and zero total field at the conducting surface) allow us to construct a scattered field of the form

$$E_z^s = E_0 \sum_{n=-\infty}^{\infty} j^{-n} a_n H_n^{(2)}(k\rho)\, e^{jn\Phi} \tag{1.4}$$

where the $H_n^{(2)}$ are Hankel functions of the second kind, and the a_n are a set of undetermined mode coefficients. The total field is simply

$$E_z = E_0 \sum_{n=-\infty}^{\infty} j^{-n} \left[J_n(k\rho) + a_n H_n^{(2)}(k\rho) \right] e^{jn\Phi} \tag{1.5}$$

Because $\psi = E_z = 0$ at the cylinder surface, the undetermined coefficients are readily found to be:

$$a_n = -J_n(ka) \,/\, H_n^{(2)}(ka) \tag{1.6}$$

The far-zone approximation to the scattered field uses a standard asymptotic form of the Hankel function (Hildebrand (1962))

$$H_n^{(2)}(k\rho) \sim \sqrt{\frac{2}{\pi k\rho}}\, e^{-j(k\rho - \pi/4 - n\pi/2)} \tag{1.7}$$

Equation 1.4 then becomes:

$$E_z^s \underset{[\rho \to \infty]}{\cong} E_0 \sqrt{\frac{2}{\pi k\rho}} \sum_{n=-\infty}^{\infty} a_n\, e^{jn\Phi}\, e^{-jk\rho} \tag{1.8}$$

and we define the far-field pattern function by the factor

analogous to a Fourier sum:

$$g(\Phi) = \sum_{n=-\infty}^{\infty} a_n e^{jn\Phi} \tag{1.9}$$

Later, in developing the inverse scattering method, we will be interested in translations of the pattern function. These may be calculated with the following relation:

$$g'(\Phi) = g(\Phi)\, e^{jk\rho_0 \cos(\Phi - \Phi_0)} \tag{1.10}$$

Here ρ_0 is the radius between the origins and Φ_0 is the angle

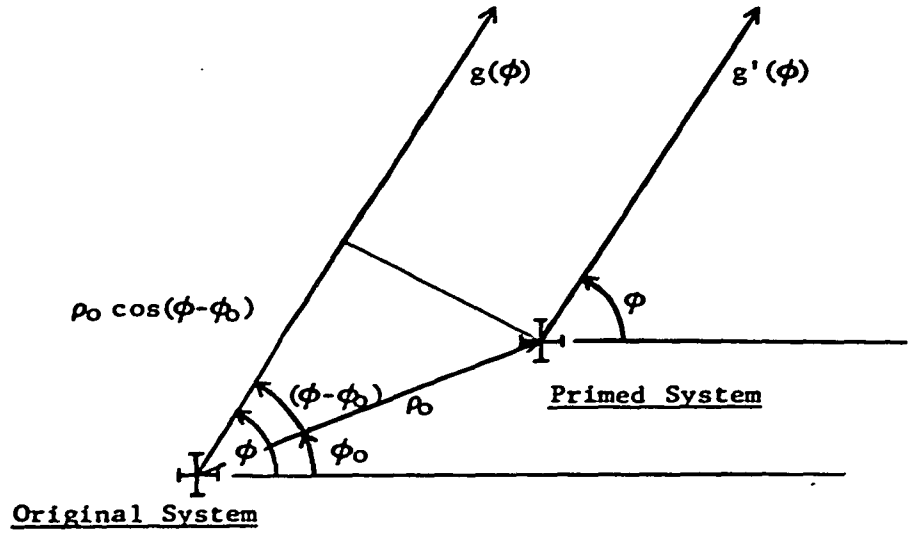

Figure 1.2 : Pattern function translation geometry. The signal from the primed system must start later by the time equal to the projection $\rho_0 \cos(\Phi - \Phi_0)$ measured in periods.

from the original to the primed system. This relationship follows from proper phase additions to a signal originating in the primed coordinate system so that it has the same behavior at infinity as

the original signal. In Figure 1.2 the signal from the primed system must start later by a time equal to the projection $\rho_o \cos(\phi-\phi_o)$ measured in periods. Therefore, as above, $g'(\phi)$ represents the signal $g(\phi)$ with the projection added as phase. The same result follows when a reverse translation is made from the primed to the original system, except $\phi_o'=\phi_o+\pi$. Consequently double translations arriving back at the first origin involve no change of $g(\phi)$.

In the primed coordinate system the pattern function $g'(\phi)$ may be Fourier analyzed in the same manner as Equation 1.9:

$$g'(\phi) = \sum_{n=-\infty}^{\infty} a_n' e^{jn\phi'} \tag{1.11}$$

and a scattered field solution can be constructed as in Equation 1.4:

$$E_z^{s'} = E_o \sum_{n=-\infty}^{\infty} j^{-n} a_n' H_n^{(2)}(k\rho') e^{jn\phi'} \tag{1.12}$$

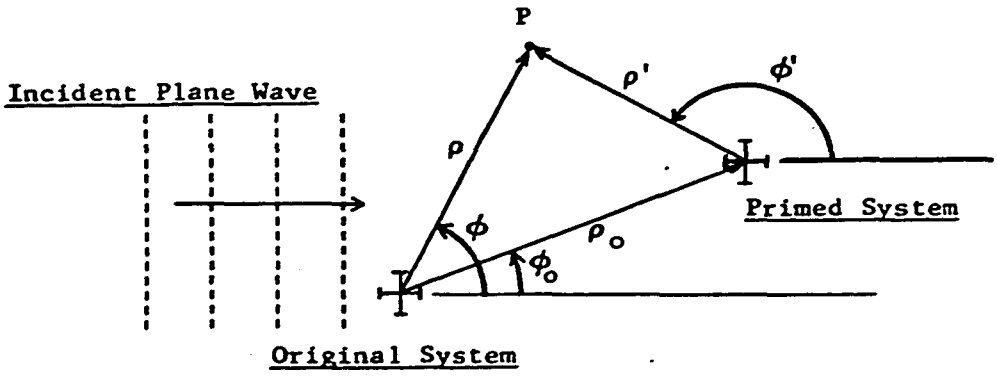

Figure 1.3 : Incident field translation geometry. The phase at P must be the same in either coordinate system. Therefore the field measured from the primed system must include the phase factor $\rho_o \cos\phi_o$ when a translation is made from the original system.

A solution for the scattered wave may be built up in the region of space beyond the minimum radius circle just enclosing the scattering object (Mittra (1970)). The total field in this region is then the sum of the incident field with respect to the primed system and the new scattered solution $\psi(\rho',\phi')$. The translated incident field is

$$\begin{aligned}\psi_{inc}(\rho',\phi') = E_z^{i'} &= E_0 e^{-jk(\rho_0\cos\phi_0+\rho'\cos\phi')} \\ &= e^{-jk\rho_0\cos\phi_0} \cdot E_z^i\end{aligned} \tag{1.13}$$

and this follows from a simple vector sum. See Figure 1.3. We now write down the total field expression for the primed coordinate system:

$$E_z' = E_0 \sum_{n=-\infty}^{\infty} j^{-n} \left[e^{-jk\rho_0\cos\phi_0} J_n(k\rho') + a_n' H_n^{(2)}(k\rho')\right] e^{jn\phi'} \tag{1.14}$$

This completes the electromagnetic theory we need for developing an inverse scattering technique for cylinders.

CHAPTER II

TECHNIQUE FOR INVERSE SCATTERING

When we look for ways to develop information about the identity of a scattering object from measurements of the scattered field, we rely upon techniques of the "inverse scattering" problem. In the present study we want to determine the location and size of a conducting cylinder. Taking the scattered far-field pattern, we regenerate the near field along azimuthal and radial contours. This theory is 2-dimensional (applicable to cylindrical structures) which is reduced in complexity by assuming an incident wave polarization parallel to the cylinder axis. For conducting cylinders normal to the reconstruction plane, this means that we have Dirichlet boundary conditions. We search for points of zero field in the near-zone and record them. Since the cylinder is a convex body, it is possible, using only the pattern function translations given by Equation 1.10, to locate surface points within the regions of valid near-field expansion (that is, within the space outside of the minimum radius circle just containing the conductor).

The first step in this inverse scattering process is a Fourier analysis of the far-field pattern:

$$a_m = \mathrm{Re}\left[\int_0^{2\pi} g(\Phi) e^{jm\Phi} d\Phi\right] + j\,\mathrm{Im}\left[\int_0^{2\pi} g(\Phi)\, e^{jm\Phi} d\Phi\right] \qquad (2.1)$$

As will be the policy regarding analysis throughout the paper, the mathematics will be in complex form for generality, although making complex measurements of a pattern function is an idealization.

This course was chosen so that the loss of reconstruction accuracy would be more method-dependent.

Once the set of Fourier coefficients is obtained, we can find the field values at any point within the range of the reconstruction method, Equation 1.5 or 1.14, depending on whether the cylinder is centered or not. The first test that can be preformed is a check of the matching of the Fourier sum to the original pattern function:

$$\int_0^{2\pi} \left\{ \left[Re(g(\Phi)) - \sum_{n=-\infty}^{\infty} (Re(a_n)\cos n\Phi - Im(a_n)\sin n\Phi) \right]^2 + \left[Im(g(\Phi)) - \sum_{n=-\infty}^{\infty} (Re(a_n)\sin n\Phi + Im(a_n)\cos n\Phi) \right]^2 \right\} d\Phi \qquad (2.2)$$

The smaller the number obtained from this operation, the more accurately the decomposition relates to the pattern function. For the cylinder, the numbers vary very quickly as translations are applied to the pattern function, but from their magnitude, estimates may be made of the reconstruction quality. We will discuss this in detail in Section 5.c.

Because we consider only the cylinder in this study, the theory as developed in Chapter 1 is sufficient for all pattern function translations. More generally, this would be true for any convex shape. We can strictly determine only those points of the scatterer which lie on the circle of minimum radius completely enclosing the body. The process of translation which allows more points to be found, as in Figure 2.1, extends the region of determinable field into the area invalid in the untranslated analysis (region I in Figure 2.1). This is known as analytic continuation (Mittra (1970)).

Non-convex bodies may be analyzed by a process involving different

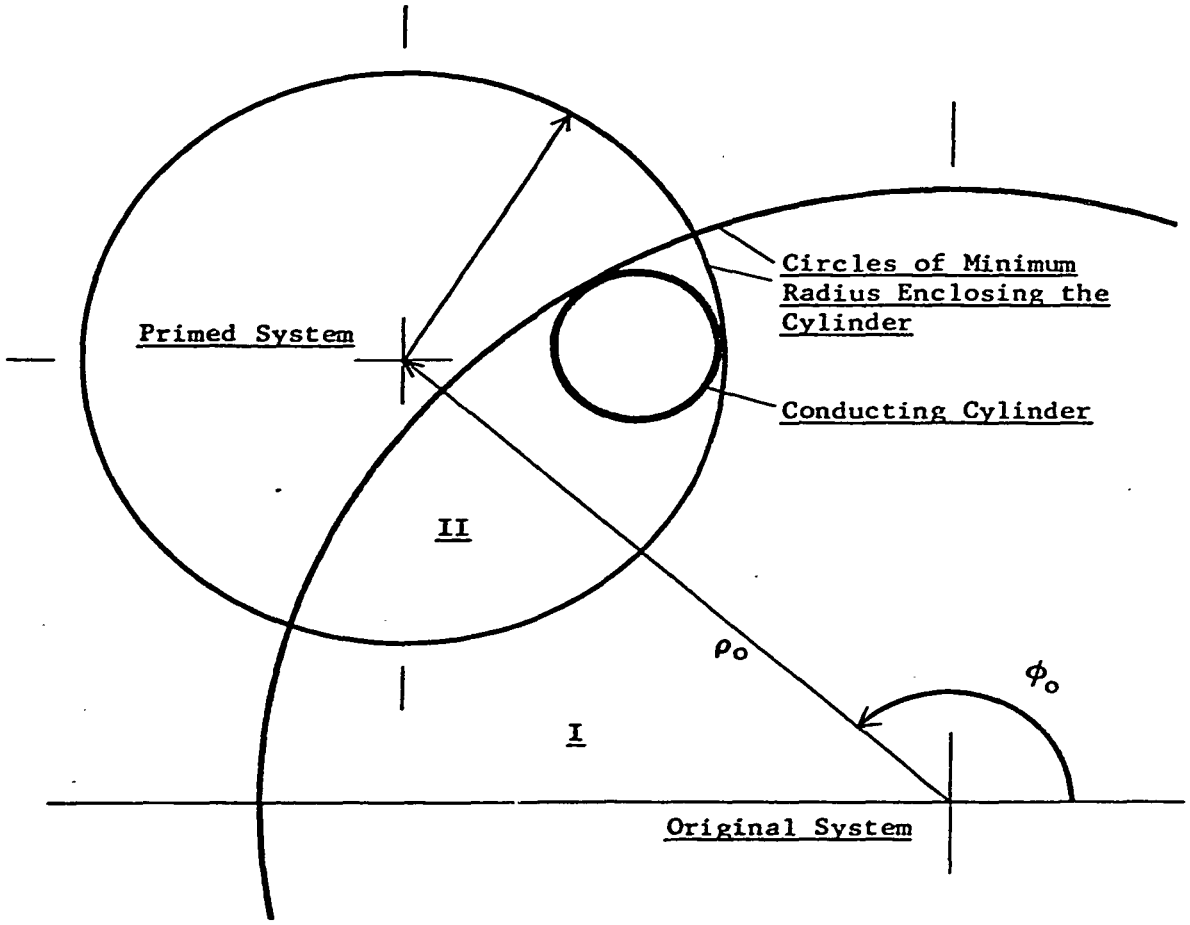

Figure 2.1 : Geometry for analytic continuation. In the original system, regions I and II are inside the circle of minimum radius enclosing the cylinder. A translation to the primed system allows computation of the field in region I, which localizes the body to region II.

expansions of the wavefunctions for the region extending from the origin to the circle of maximum radius just excluding the body. This is explored by Imbriale and Mittra (1970), and is not of interest in the present study.

CHAPTER III

METHOD FOR COMPUTATION

For this study, we chose a group of cylinder sizes within the range of practical microwave experimentation. Radii varied from 0.25λ (ka=1.57) to 4.0λ (ka=25.12). See Figure 3.1. A complex

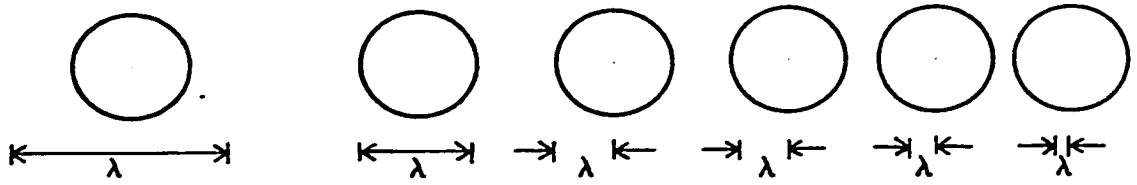

a=0.25λ	a=0.50λ	a=1.0λ	a=1.1λ	a=2.0λ	a=4.0λ
ka=1.57	ka=3.14	ka=6.28	ka=6.91	ka=12.56	ka=25.12

Figure 3.1 : Diagram showing the relationship between wavelength and radius for the cylinders studied in these reconstruction experiments.

function subprogram HANK (Howarth (1970)) was used to compute the values of $H_n^{(2)}$, the Hankel function of the second kind, and the initial set of Fourier coefficients a_n was constructed as:

$$a_n = -\text{Real (HANK(n,ka))/HANK(n,ka)} \qquad (3.1)$$

with k the wavenumber and a the radius.

Pattern functions generated from this set of coefficients were tabulated at 3^o intervals from -180^o to $+180^o$, a scheme which parallels the discrete measurement scheme of a laboratory experiment, although the interval was chosen to satisfy a one-page output requirement and a consideration of computational necessity. See

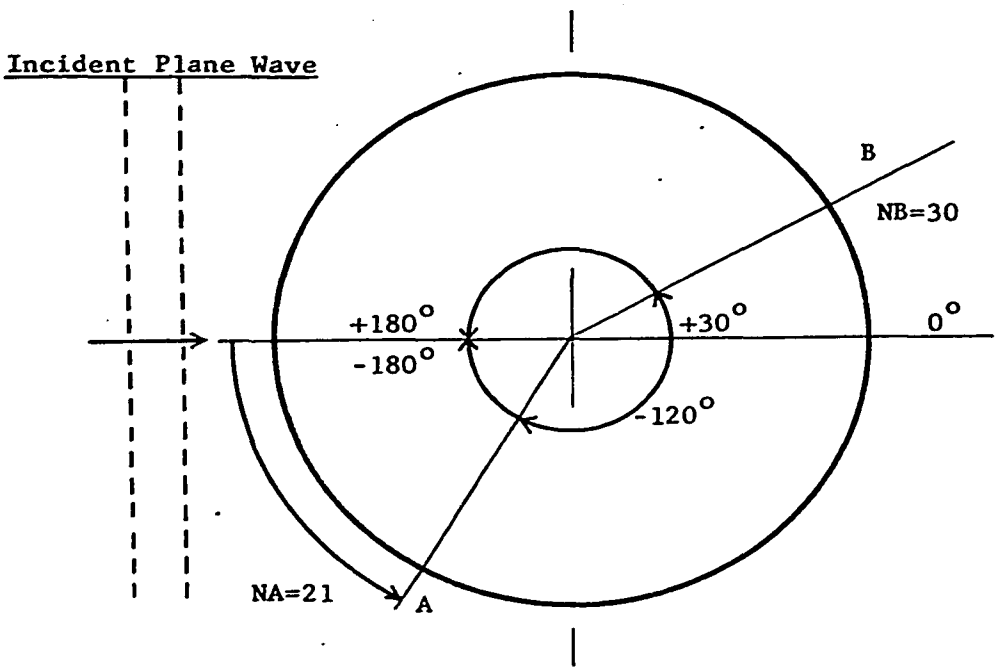

Figure 3.2 : Representation of angles in the azimuthal reconstruction process. The plane wave is incident from the left. A is the direction to a reconstructed field point, and in the program is measured in integral units of 3°, with NA=1 for -180° and NA=121 for $+180^{\circ}$. B is the direction of a translation, measured as an integer from 0°.

Figure 3.2 for the angular measurement plan. In Chapter 4 we will discuss the a priori, or structural, information aspects of this scattering problem, and we will see that a ka=6.28 cylinder has four pairs of degrees of freedom, meaning that the radiation is equivalent to four complex oscillators. From this, 121 data points for 360° indicates 30 data points for each pair of degrees of freedom, a good prediction for accuracy.

The most important differences between the theory explained in Chapter 1 and any computational scheme based on it are the

limitations on the number of terms in the sums, and the error introduced in numerical procedure. The inverse scattering programs accepted as input data the tabulated far field pattern function

$$GPHI(I) = \sum_{m=-15}^{+15} a_m \, e^{j m ((3I-183)\cdot \frac{2\pi}{180})} \Bigg|_{I=1}^{I=121} \qquad (3.2)$$

corresponding to Equation 1.9. With these limits, the input pattern function for cylinders as large as 1.1λ radius was built from a set of Fourier coefficients which included all those non-zero to 6 decimal places. See Figure 3.3. Aspects of reconstruction degradation due to the coefficient limitations will be discussed in Chapter 5.

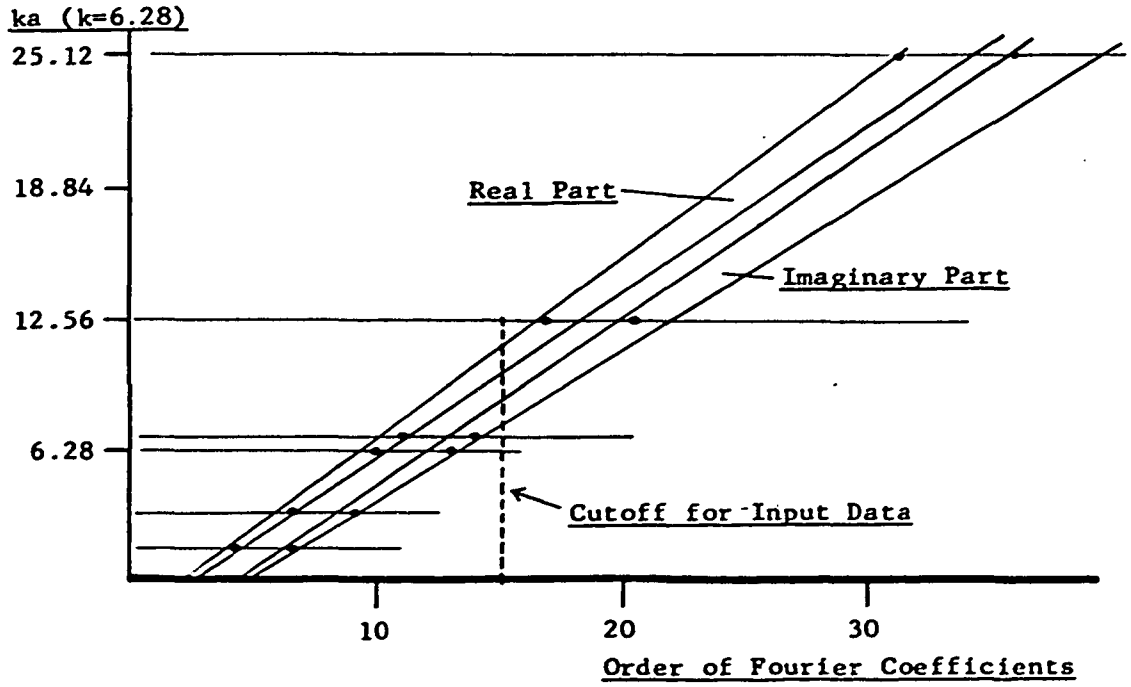

Figure 3.3 : Diagram showing the order necessary to include all non-zero 6 decimal place Fourier coefficients. Note that if n is the order, the total number of complex coefficients involved is 2n + 1.

The generation of Fourier coefficients and the subsequent construction of a pattern function whose values are complex numbers raises a question about possible measurement schemes, since a practical measurement of the far-field yields only an amplitude pattern unless certain special things are known, for example, the phase of the radiated signal and the precise trajectory of the measuring device with respect to the radiating object. To make an amplitude measurement you need only be in the far-zone with a reasonably accurate distance and direction figure, while the phase measurement requires distances precise to a fraction of a wavelength. Since one can never make true microwave far-field measurements in the laboratory, the complex (phase-containing) far-field pattern figures generated by the Bessel function theory contain more information than a real experiment might. But for this analysis we should use the complex figures rather than their magnitude alone, because the purpose of the study is to judge how the method itself brings about inaccurate reconstruction results.

Quite simply, the reconstruction program takes the pattern function and generates a set of Fourier coefficients that reproduce it. The bulk of the program is a series of tests, checks, and methods for preserving numerical accuracy, and a sequence of near-zone field magnitudes are plotted according to either an azimuthal or radial plan. Interpretation of these graphs results in information about the scattering object.

Translations of the pattern function, to represent the far-field

pattern of a cylinder moved away from the origin, are computed using the method of Equation 1.10. A subroutine TRANSG preforms the operation on the 121 point data set. Translation parameters involve only the radial distance and angle between the old and new coordinate systems.

The reconstruction of the a_n from the pattern function uses a more detailed set of data, where the normal group of 121 points has been enlarged to 361 by an interpolation subroutine EXPAND. Presumably this causes a better fit in regions of rapidly varying pattern function values. The reconstruction accuracy check described by Equation 2.2 is tested in a subroutine VARIA, which works with the new a_n and the original 121 point set of pattern data. No attempt was made at using the VARIA criterion as the basis of an optimization scheme for the a_n, although such a technique might be developed by treating the number returned by VARIA as a function of the a_n vector and finding a local minimum by an iterative process.

The limits of the regenerated Fourier coefficients present little problem for on-axis scattering, since there is perfect reconstruction to the 4^{th} or 5^{th} decimal place, and coefficients originally zero are regenerated as 0.000000 or $\pm$0.000001. If the field is being reconstructed near the conducting surface, such numbers can be omitted. Once translations are made, however, the order of coefficients necessary for such accuracy goes up very quickly. For the 0.25λ radius cylinder, a Fourier coefficient order of 4 provides good on-axis reconstruction. A translation of 0.05λ makes it necessary to use an order of 6 to include the significant

coefficients, even though this system fits within a circle of 0.30λ radius. An order of 6 is sufficient for a centered 0.50λ radius cylinder. This matter is treated quantitatively in Section 5.c. It should be noted here that a Fourier coefficient order of 6 implies a coefficient vector of dimension 13, to include the +,-, and zero orders. Figures in the programs use the vector dimension rather than the single-sided order.

Two types of output scans are used, the radial and the azimuthal, and an attempt was made to automate the location of scatterer points with the azimuthal scans. The field in the near-zone is reconstructed for successively smaller rings, and once a field value less than a particular cutoff is found, the program sequences the radii to the smallest circle just containing the scatterer. This works well for on-axis cylinders, but for the other cases, false zeros and inaccuracies cause it not to be worth the effort. Radial scans provide a better sort of information, as can be seen from Figures 5.e.2 and 5.e.3, but they require more initial guesswork in setting up the off-axis problem. A unit circle 3.5 units from the origin subtends only 30° of arc.

All programs and subroutines used for this study are listed in the Appendix.

CHAPTER IV

INFORMATION CONCEPTS

Any practical method of inverse scattering must make reference to a spatial information theory, since the process of reconstruction from a set of sampled points is statistical. Furthermore, since we expect to recover scattering object detail, the wavelength of the incident test field must be considered with respect to the object dimensions. Perhaps this is most easily explained by repeating an analogy due to Sir Arthur Eddington, as quoted by Gabor (1961): "If an icthyologist casts a net with meshes two inches wide for exploring the life on the ocean, he must not be surprised if he finds that 'no sea creature is less than two inches long'". Gabor (1946) and MacKay (1950) were among those primarily responsible for the development of quantal information concepts, and Gabor's earlier paper was the foundation for the extensive communications applications by Shannon (1948,1949). Of particular interest to this study, Gabor dealt with the information content of light beams, and his method for calculating the number of degrees of freedom in them can be directly applied to the scattering problem.

Recently, Winthrop (1971) has developed a pseudopotential theory for the propagation of structural information (the a priori information which comes from a knowledge of the degrees of freedom) and this seems that it will outline methods for the more complete analysis of diffraction and scattering problems. Relationships

about the structural information at different cross-sections of the field are found by the introduction of an information flow vector. Tubes of information flow are then postulated as being perpendicular to the surfaces of constant pseudopotential, in much the same way that field lines run normally between electrostatic equipotential surfaces. The theory has analogies to Huyghens' constructions and fluid mechanics, and perhaps fluid models can be used to analyze situations too complicated for the pseudopotential theory itself. However, to begin with, we must address ourselves to the points where these ideas may be of use in the present study.

The idea of quantified information and the use of "missing information" enables the communications engineer to set design characteristics and analyze the behavior of his systems, because he is dealing with a probabilistic process that has both structural and metrical aspects: he expects messages within a certain codeset, and his receiving equipment is designed to discriminate within the expected range of frequency, voltage level, phase, and so forth. In electromagnetic theory, the precise description of certain quantities, such as ϕ and $\nabla\phi$, leads to a complete exact solution for the fields involved. In this case the a priori (structural) information results from a knowledge of the geometry and the physical laws. On the other hand, a specification of the properties in a specific area of the field usually does not lead to a solution which describes the remainder of the field and its sources. The inverse scattering problem is beset with this difficulty, and we must therefore find a way to associate field information with

bounds on solution precision: bounds that vary with the initial information. We will then be able to investigate with more precision such problems as the calculation of points in the far-field from select near-field points. In particular, it may help make unnecessary the 360^{o} measurements required for accurate Bessel function analysis by providing confidence in the accuracy of discrete systematic measurement patterns suited to Cartesian recording equipment.

Besides sampling, there is another way information concepts may be applied. A scattering system may be considered as a state space, and using analogies to statictical mechanics, we can work from the fundamental invariant

$$\text{Entropy} + \text{Information Content} = \text{Constant} \qquad (4.1)$$

(MacKay (1950)), which is simply the relationship between unstructured and structured knowledge within a set of boundary conditions. In form it expresses the yin-yan principle that what we know plus what we don't know about the system defines the whole (sometimes with a little of the second in the first and vice-versa, too!). The two sub-classes of information, the structural (a priori) and information from measure (a posteriori) can then be acted upon to change the entropy (disorder).

Quantities of information on structure for light beams (and electromagnetic waves in general) are directly related to the degrees of freedom for a system (MacKay (1950)). For a monochromatic beam, their number may be calculated from the relation derived

by Gabor (1961):

$$F = 2 \times 2 \times \text{Object Area} \times \text{Accessible Fourier Area} \qquad (4.2)$$

where the first 2 accounts for the complex nature of the optical disturbance, and the second for polarization. In the cylindrical scattering problem, both 2's are suppressed because we wish to talk of numbers of oscillators (themselves complex) and because the axial polarization never introduces a transverse electric field. To keep matters clear, we will always use the terms "complex" or "pairs" when referring to an equivalent number of oscillators and the associated degrees of freedom.

For the two-dimensional scattering problem, the calculation of the number of degrees of freedom must account for a difference in system orientation from the light-beam case: the object area and Fourier transform space are one-dimensional. From any direction in the two-dimensional space of the cylindrical scattering problem, the object area is the diameter 2a. The maximum accessible Fourier area is then the diameter of the circle of radius η/λ, where η is the refractive index. With only the axial polarization considered,

$$N = 2a \times 2\eta/\lambda \qquad (4.3)$$

is the number of oscillators necessary for an equivalent radiation pattern. We can verify the validity of this figure with the following thought about sampling theory: scattering by an object $\frac{1}{2}\lambda$ in diameter can provide no information about the object detail. From

actual practice, we know that in scattering problems this size object can be replaced by a single line of current, or one oscillator. Therefore, when $a=\frac{1}{2}\lambda$ and $\eta=1$,

$$N = 2\lambda/4 \times 2/\lambda = 1 \qquad (4.4)$$

we find that we have indeed provided the correct number of complex degrees of freedom. For the cylinder sizes discussed in this study, Table 4.1 shows the tabulations from Equations 4.2 and 4.3. Some application of these numbers is found in Section 5.d, where reconstruction from sectors of pattern function data is treated.

Cylinder Radius a	Number of Oscillators N	Number of True Degrees of Freedom F
$a=0.25\lambda$	N=1	F=2
$a=0.5\lambda$	N=2	F=4
$a=1.0\lambda$	N=4	F=8
$a=1.1\lambda$	N=4.4=5	F=8.8=9
$a=2.0\lambda$	N=8	F=16
$a=4.0\lambda$	N=16	F=32

Table 4.1 : Relationship between cylinder size, number of degrees of freedom, and equivalent number of oscillators for the inverse scattering study.

To the extent that it is found here, information theory provides some assurance that the experiment is being conducted properly. It is hoped that the ideas may find application beyond sampling, and that the behavior of diffracting and imaging systems can be numerically tied together with ubiquitous field effects, such as the nulls and Airy rings.

CHAPTER V

RESULTS OF THE INVESTIGATION

Five aspects of the reconstruction problem were studied, and they are each treated under their own subheading in this chapter. However, before proceeding it is necessary to scale a particular coordinate system extensively used in the following sections. The azimuthal field reconstructions are in real space; so the distance from -180^{o} to $+180^{o}$ is a function of the radius, $2\pi r$. Presenting these graphs in their true scaled form was considered confusing, so the alternate form of Figure 5.1 was chosen. The

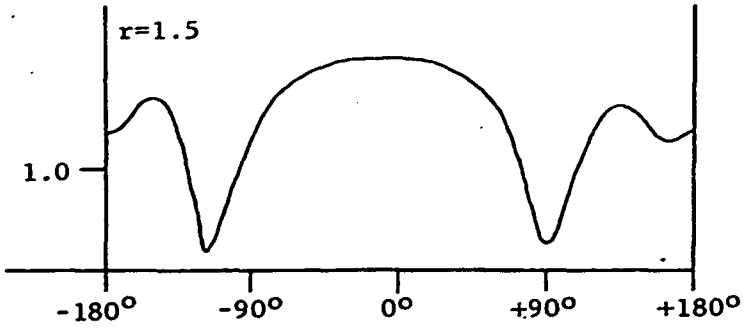

Figure 5.1 : Coordinate system for azimuthal field plots.

horizontal scale runs from -180^{o} to $+180^{o}$, and the radius is indicated in the upper left-hand corner. The vertical scale marker indicates a field magnitude of 1.0, the magnitude of the incident plane waves. If one wished to construct a graphic model of the field, the horizontal scale would have to be expanded in proportion to the radius.

5.a : Field Reconstruction for Centered Cylinders.

The diagrams in Figure 5.a.1 show a sequence of reconstructed field magnitudes for scattering by a 4.0λ radius cylinder. As the radius approaches that of the cylinder itself, the field settles to zero, indicating a returned conducting surface. Because the pattern function for this cylinder does not contain complete information (see Figure 3.3), there is in the field a periodicity which is associated with the Fourier coefficient order. However, the reconstruction is approximate (see Figure 5.b.4), and so the features of the returned field may be noted. Close to the ±180° positions at r=4.25, a peak in the standing wave is evident. This is expected since a small portion of the cylinder reflects the incident wave like a nearly plane surface. In the 0° direction, the average of the field is a minimum, indicating the shadow region of the cylinder.

Figure 5.a.2 shows a sequence of azimuthal field reconstructions for a 1.1λ radius cylinder. Now the reconstructions are in the "good" (r=2.60; r=2.10) and the "very good" regions shown in Figure 5.b.4. Again, as the radius of the reconstruction circle approaches the cylinder radius, the magnitude becomes a smooth function which settles to zero. Reconstruction for radii less than the cylinder radius briefly appears to be symmetric with that for radii above it, but, in diagrams not shown, rapidly expands into saturation by r=0.5. The feature of the drifting peaks in the sequence simply represents a geometrical phenomenon: as the radius decreases the circular contour intersects fewer standing

waves about the cylinder.

The pattern function data is altered for the reconstructions shown in Figure 5.a.3. These new pattern functions represent measurement data that might be supplied by increasingly less accurate equipment (6 decimal place accuracy is beyond the limit of practicality for normal equipment). We see that these degradations do not affect reconstruction at r=1.60, but that the data accurate to 2 decimal places causes inaccurate reconstruction at radii less than this.

Noise added to the pattern function data provides the reconstructions in Figure 5.a.4. Again, except for noise with σ=0.05, the changes do not affect reconstruction at r=1.60. However, even the noise with σ=0.0005 affects reconstruction at r=1.10 although the field behavior is obvious at this noise level. We may conclude that reconstruction will be accurate with pattern function data good to 3-4 decimal places.

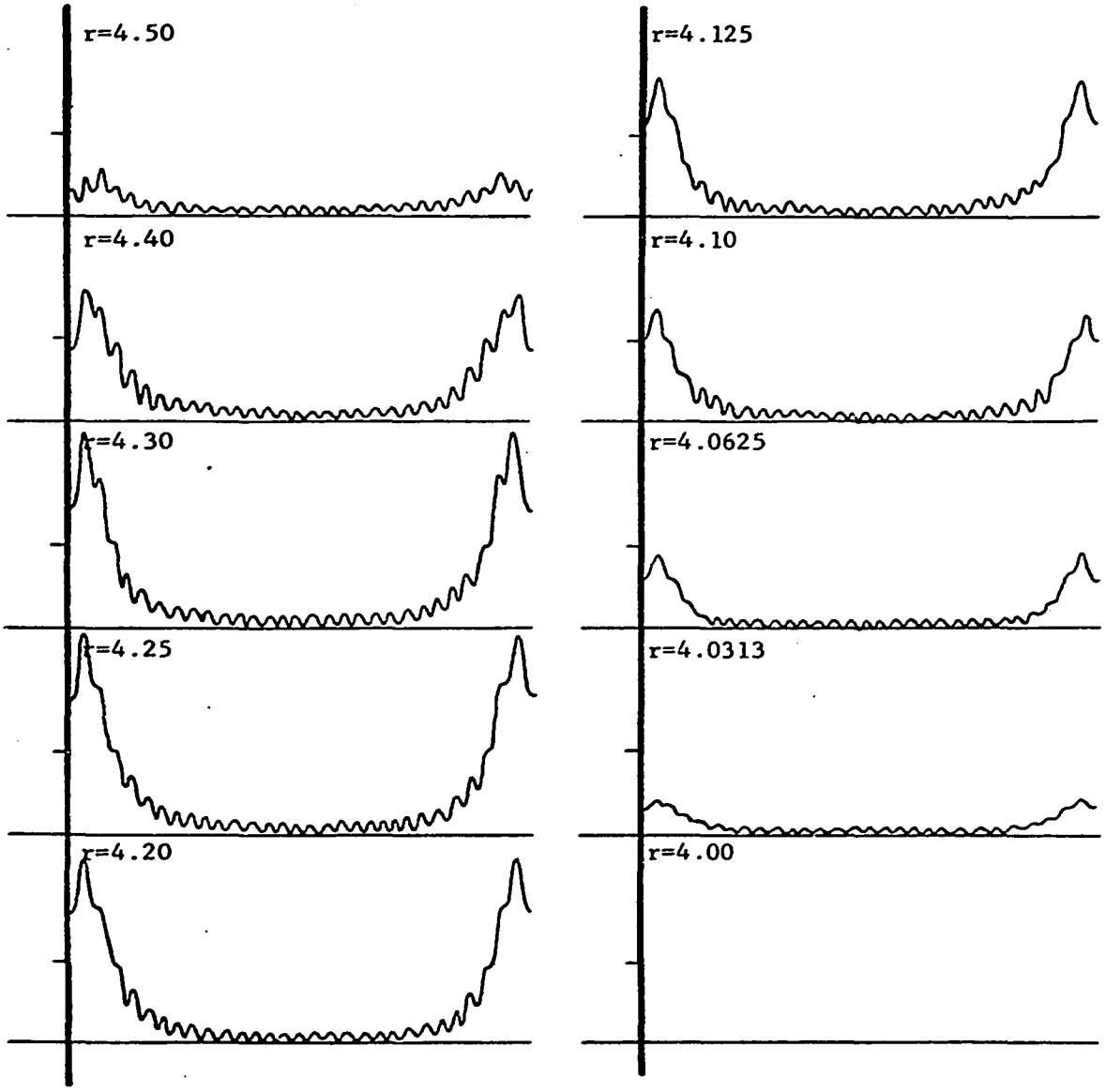

Figure 5.a.1 : Sequence of azimuthal field reconstructions for the 4λ radius cylinder. The Fourier coefficient order is 15. Note the standing wave peak at r=4.25.

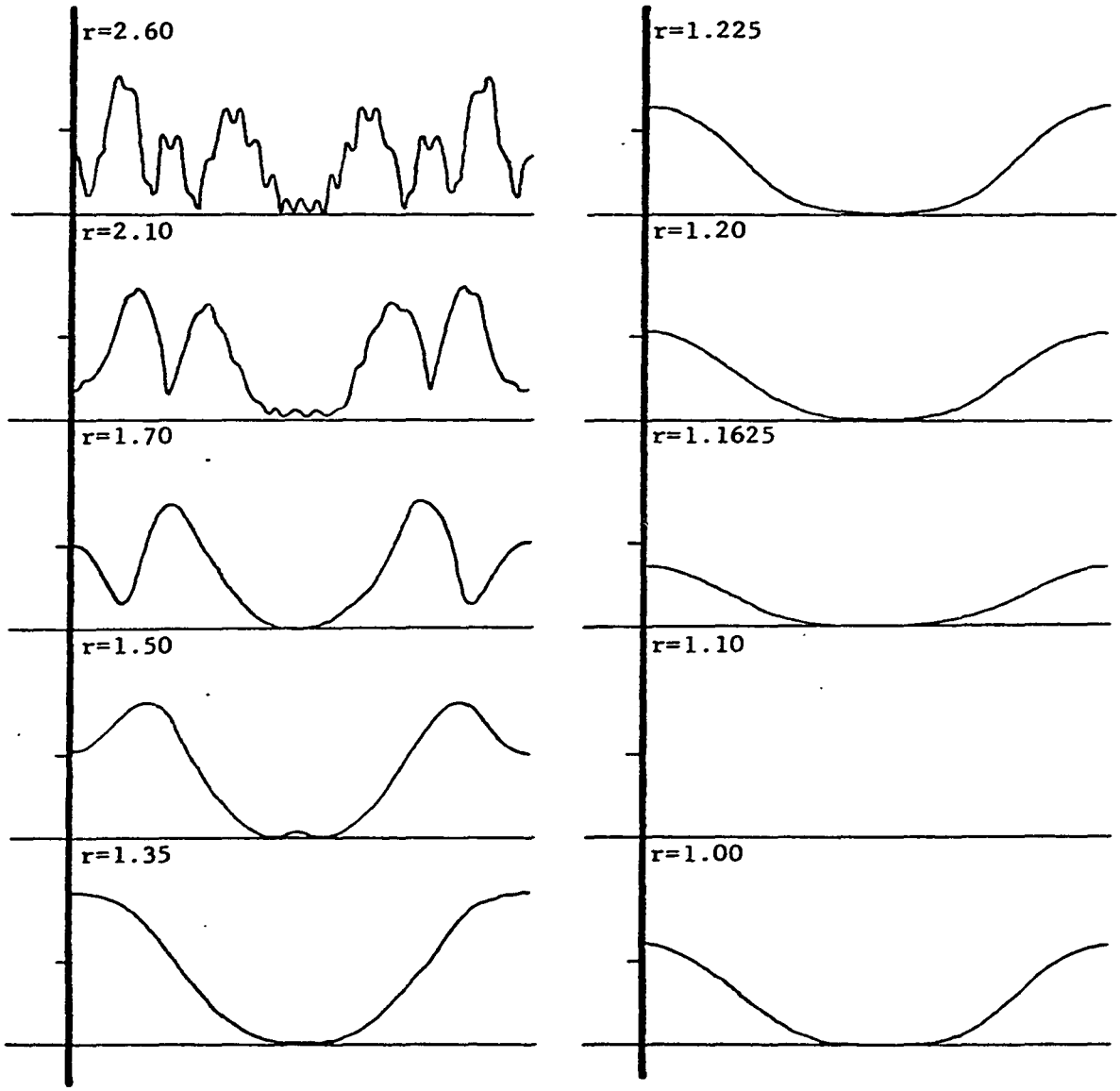

Figure 5.a.2 : Sequence of azimuthal field reconstructions for the 1.1λ radius cylinder. The Fourier coefficient order is 15.

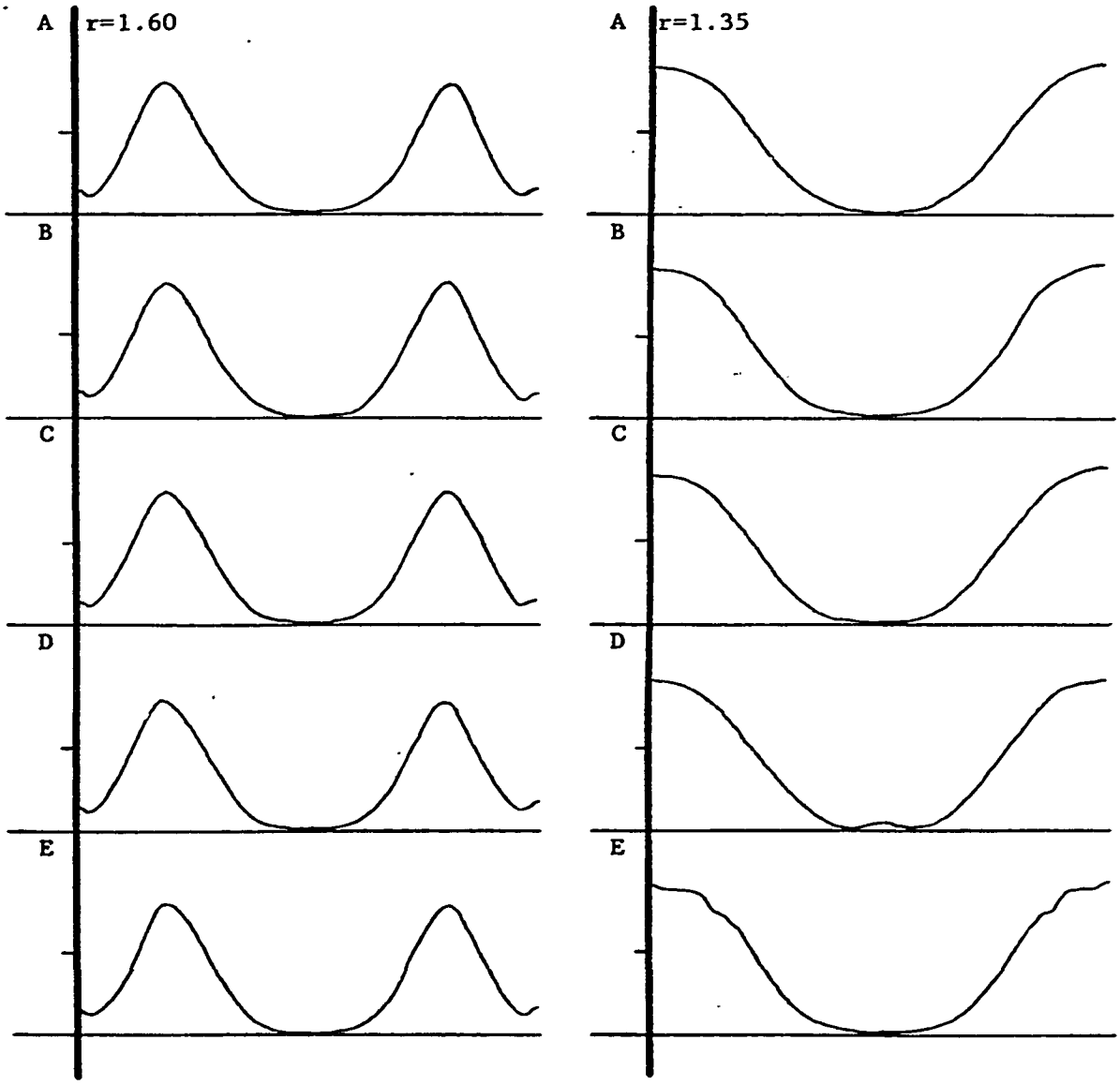

Figure 5.a.3a : Azimuthal field reconstructions for the 1.1λ radius cylinder. The Fourier coefficient order is 15, and the reconstruction is at r=1.60 (left) and r=1.35 (right).
Cases: A. Original 6 decimal place data.
B. Roundoff to 4 decimal places.
C. Truncation to 4 decimal places.
D. Roundoff to 2 decimal places.
E. Truncation to 2 decimal places.

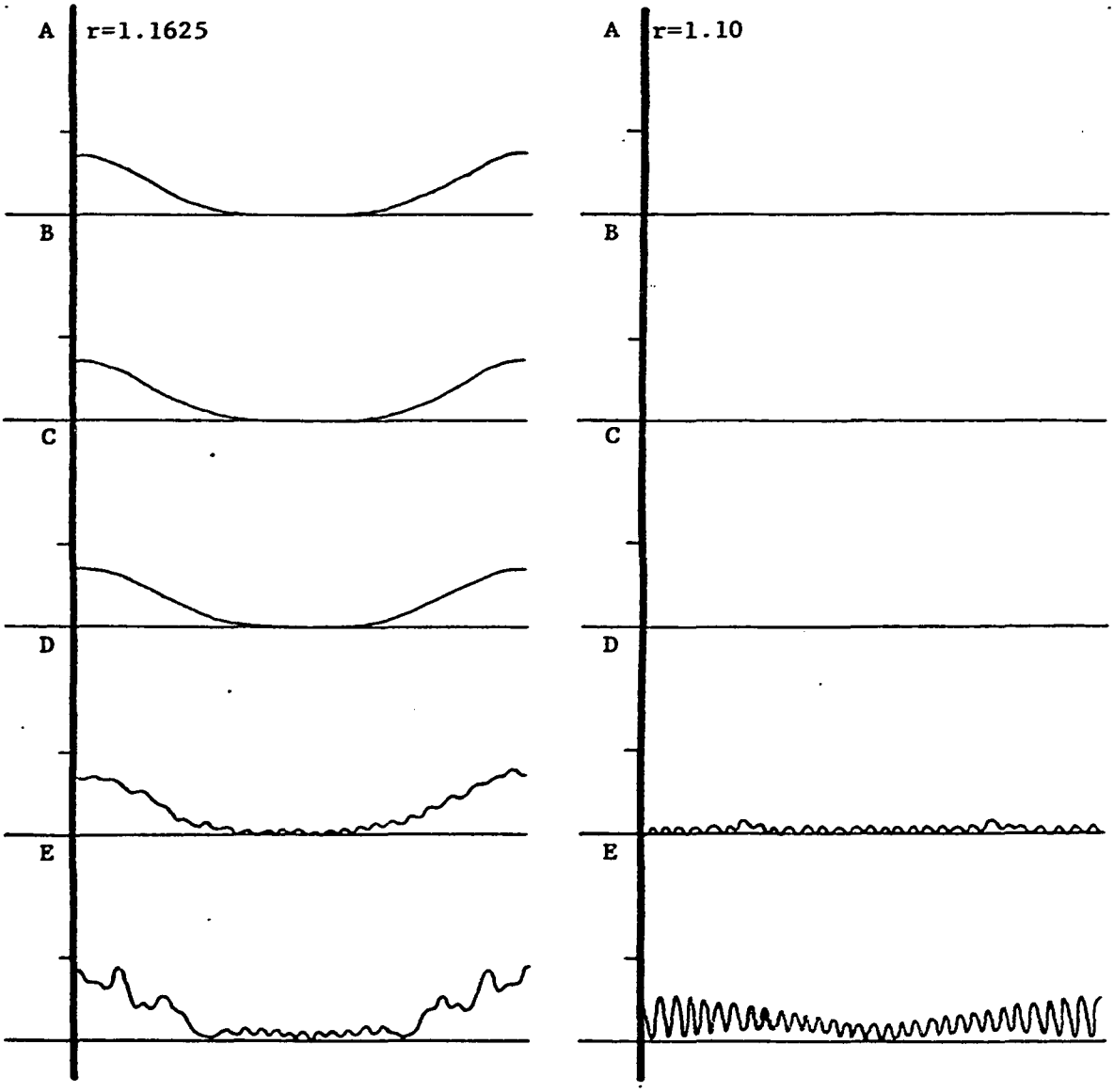

Figure 5.a.3b : Azimuthal field reconstructions for the 1.1λ radius cylinder. The Fourier coefficient order is 15, and the reconstruction is at r=1.1625(left) and r=1.10(right).
Cases: A. Original 6 decimal place data.
B. Roundoff to 4 decimal places.
C. Truncation to 4 decimal places.
D. Roundoff to 2 decimal places.
E. Truncation to 2 decimal places.

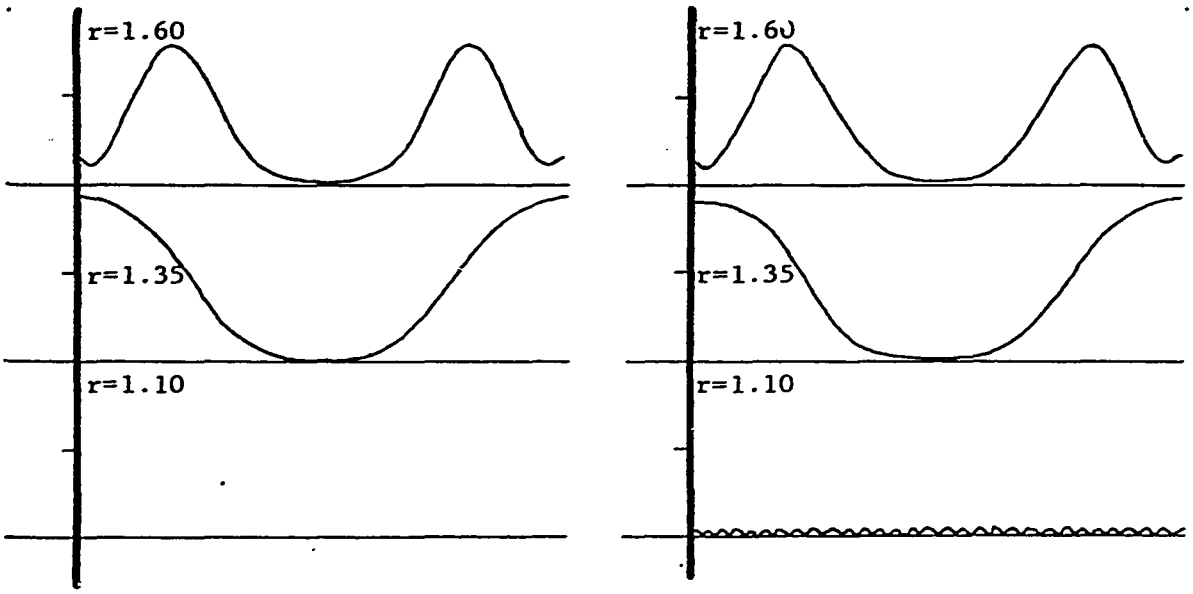

Figure 5.a.4a : Azimuthal field reconstruction for the 1.1λ radius cylinder. The Fourier coefficient order is 15.
Cases: Left. Original 6 decimal place data.
Right. Gaussian noise added. μ=0.0, σ=0.0005.

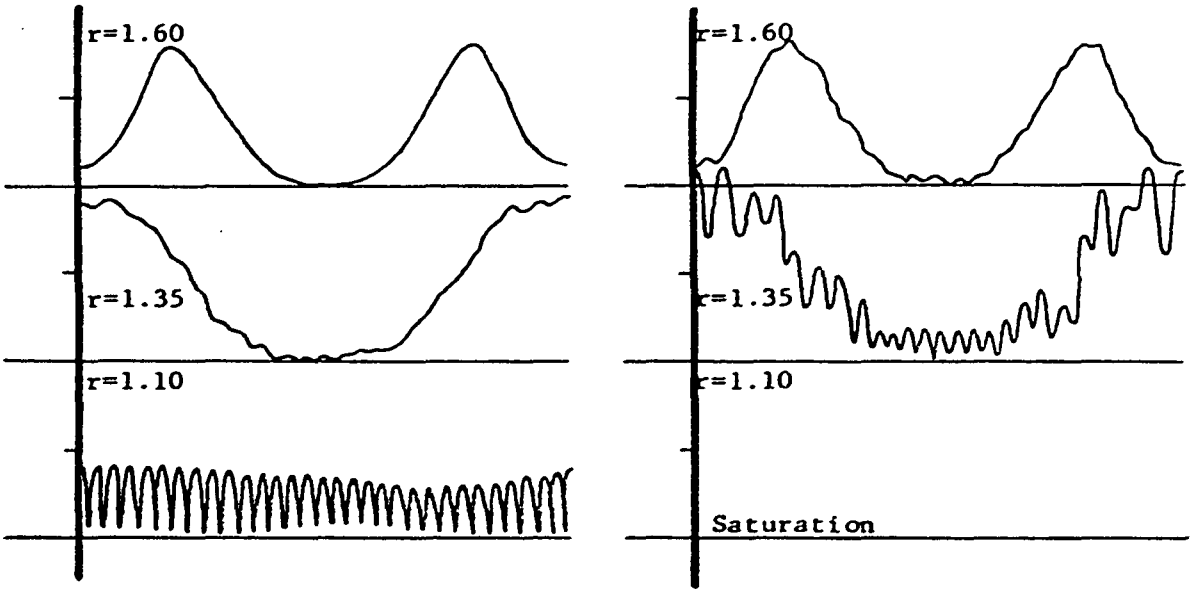

Figure 5.a.4b : Azimuthal field reconstruction for the 1.1λ radius cylinder. The Fourier coefficient order is 15.
Cases: Left. Gaussian noise added. μ=0.0, σ=0.005.
Right. Gaussian noise added. μ=0.0, σ=0.05.

5.b : Fourier Coefficient Orders.

Calculating the near-field while changing the limits of the Fourier sum provides information about accurate and inaccurate reconstruction. In Figure 5.b.1 the reconstructed field for a 1.0λ radius cylinder is shown at several radii for three different Fourier coefficient orders. At r=3.0 and r=1.5 the order 5 reconstruction contains no real information, while the order 10 plot looks first like a highly degraded, and then a slightly degraded version of the expected field. At r=3.0 the order 15 reconstruction is approximate, and at r=1.5, it is very good. As the radius of the conducting surface is approached, all three limits provide good results.

Reconstructions for a 0.25λ radius cylinder are found in Figure 5.b.2. At r=8.0 there is nothing believable about the returned field for any of the coefficient orders. At r=1.0 the order 7 and order 15 reconstructions are similar, with the latter appearing to be the best choice. At r=0.75 the order 7 plot seems best, while the order 15 reconstruction is just beginning to blow-up. As r approaches 0.25 the order 3, 5, and 7 reconstructions provide good results, while the order 15 plot has saturated.

These observations bring out an important detail which may be converted into a criterion on the Fourier coefficient order necessary for good computation of the reconstructed fields. The best angular resolution for a circular pattern is related to the order of the Fourier sum, and the best linear resolution along the circumference is related to the angular resolution. Doubling

the radius doubles the circumferential length, so a detail of specific length on each circle requires a higher Fourier coefficient order to resolve it on the larger one.

For plane wave scattering, we may approximate the Fourier coefficient order necessary for reconstruction at any radius by determining the percentage of the circumference intercepted by 360^{o} phasefronts at the point they are nearly normal to the circle. See Figure 5.b.3. This defines the region of greatest angular variation. Provided the radius is greater than the wavelength, the chord B and arc A are nearly equal. Therefore,

$$n=2\pi r/\lambda \qquad (5.b.1)$$

is a measure of the circumference in terms of arc length, and should be the Fourier coefficient order necessary to reproduce a circular function whose greatest angular frequency has an arc period A.

In Figure 5.b.4, one of the important results of this study, the above criterion is plotted together with bounds on the range of good reconstruction, a composite of the information from this section and Section 5.e. We see that the criterion of Equation 5.b.1 coincides with the upper bound. Further studies can make use of this in order to be within a region of good reconstruction at any specific distance from the origin.

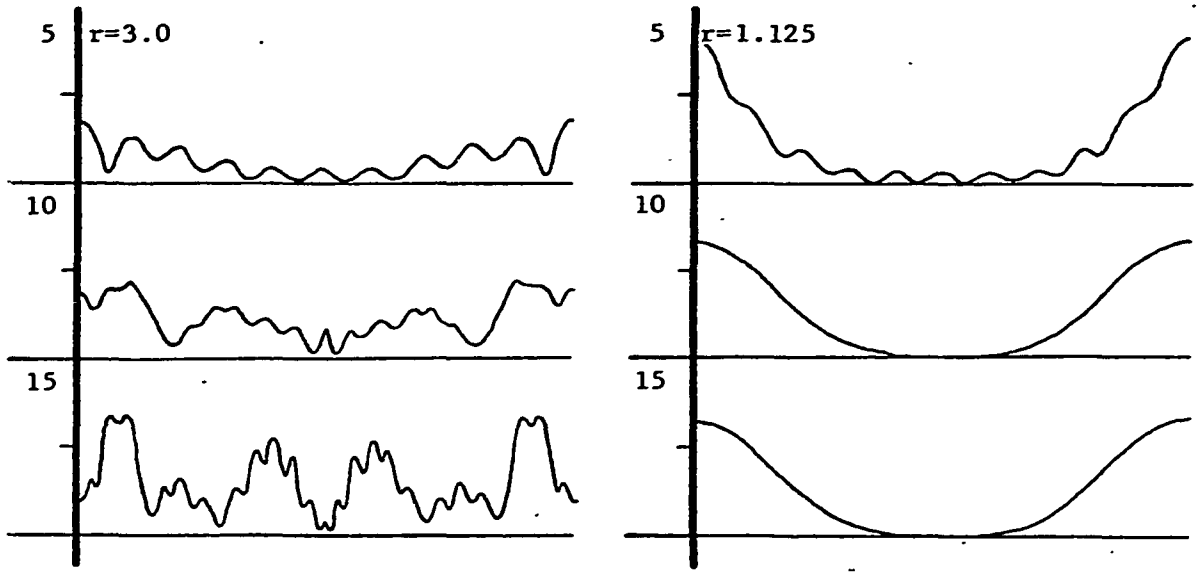

Figure 5.b.1a : Azimuthal field reconstructions for a 1.0λ radius cylinder at r=3.0 (left) and r=1.125 (right). The Fourier coefficient order is indicated in the diagram.

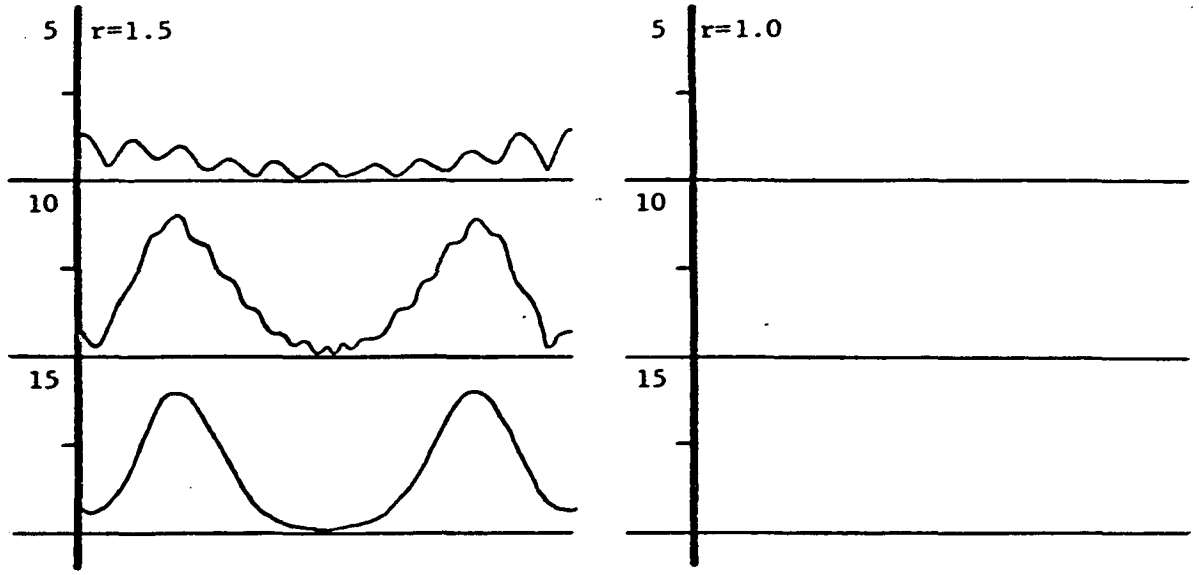

Figure 5.b.1b : Azimuthal field reconstructions for a 1.0λ radius cylinder at r=1.5 (left) and r=1.0 (right). The Fourier coefficient order is indicated in the diagram.

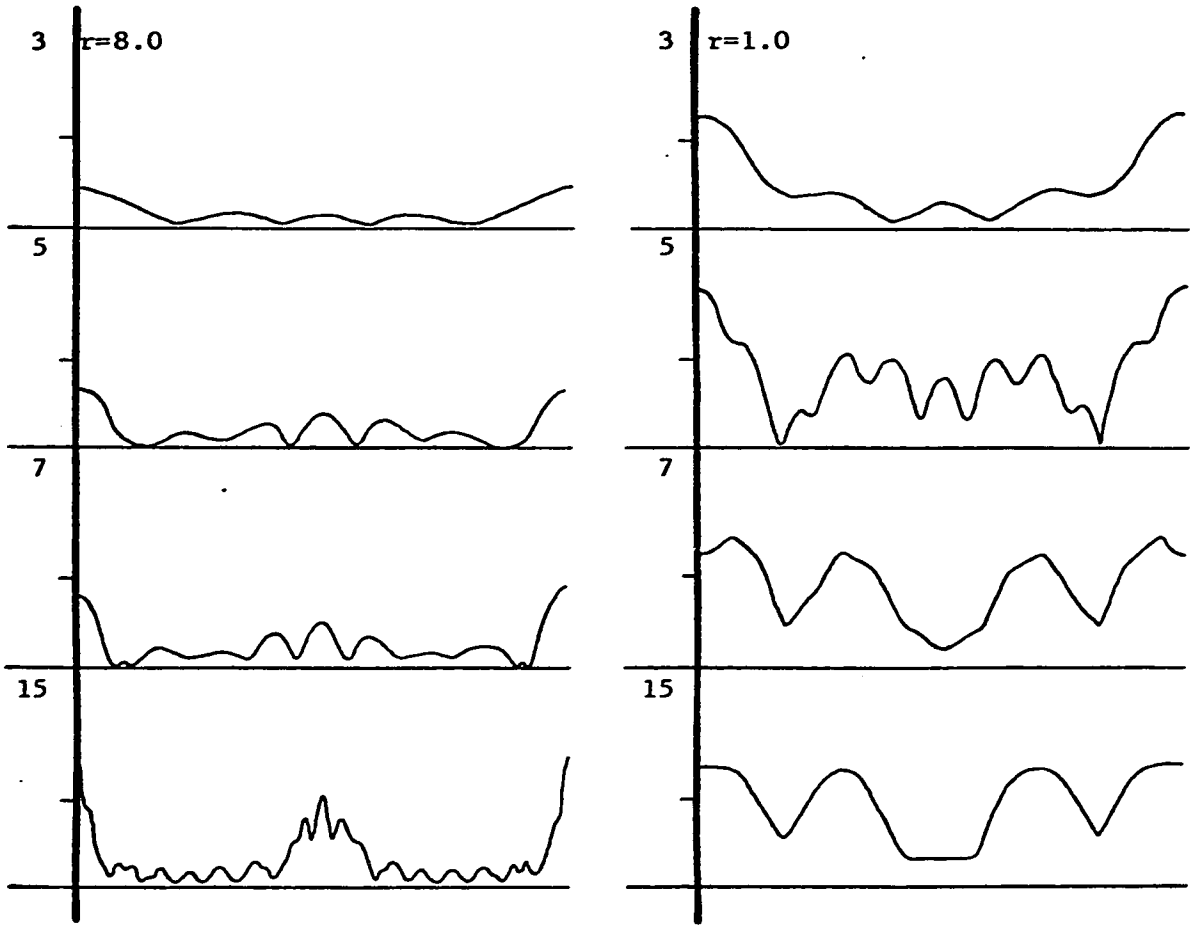

Figure 5.b.2a : Azimuthal field reconstructions for the 0.25λ radius cylinder at r=8.0 (left) and r=1.0 (right). The Fourier coefficient order is indicated in the diagram.

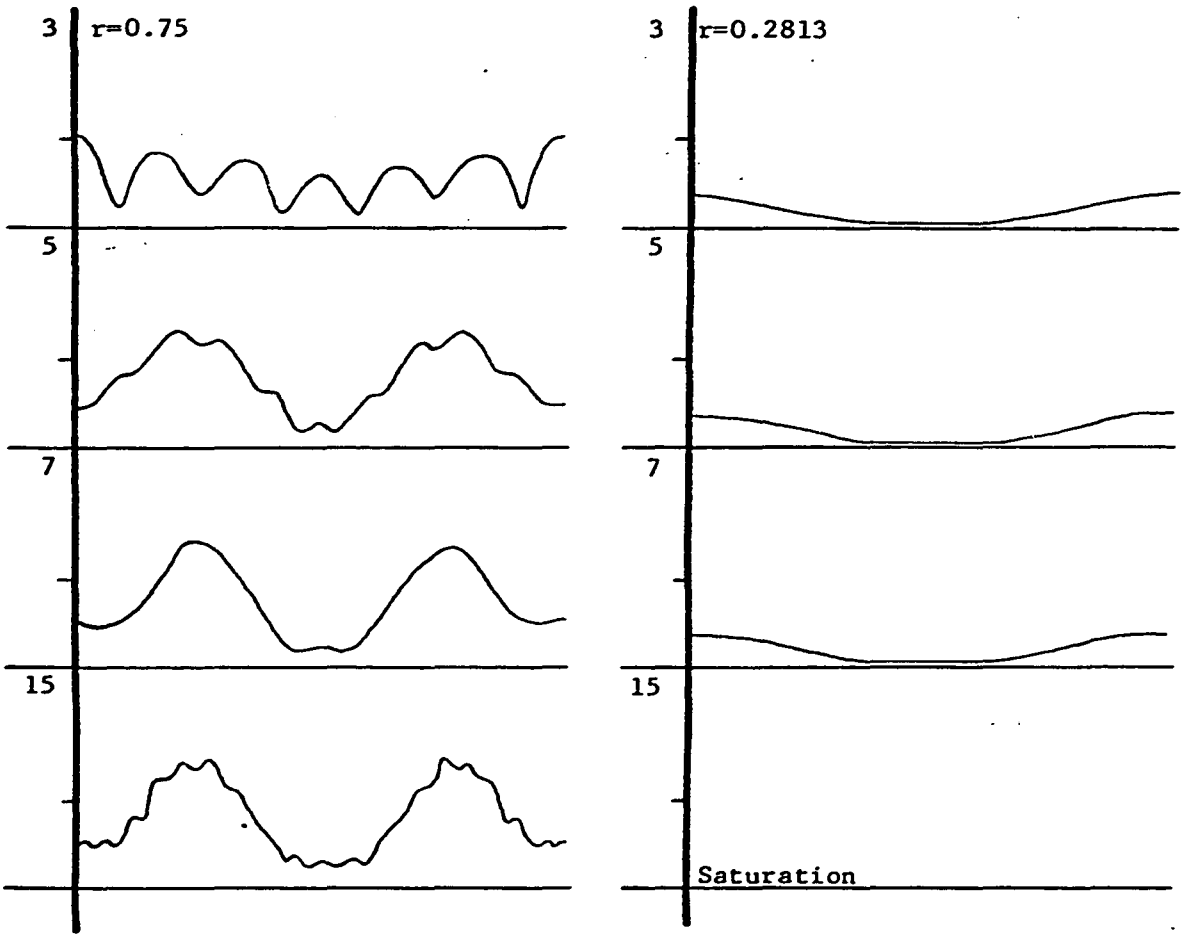

Figure 5.b.2b : Azimuthal field reconstructions for the 0.25λ radius cylinder at r=0.75 (left) and r=0.2813 (right). The Fourier coefficient order is indicated in the diagram.

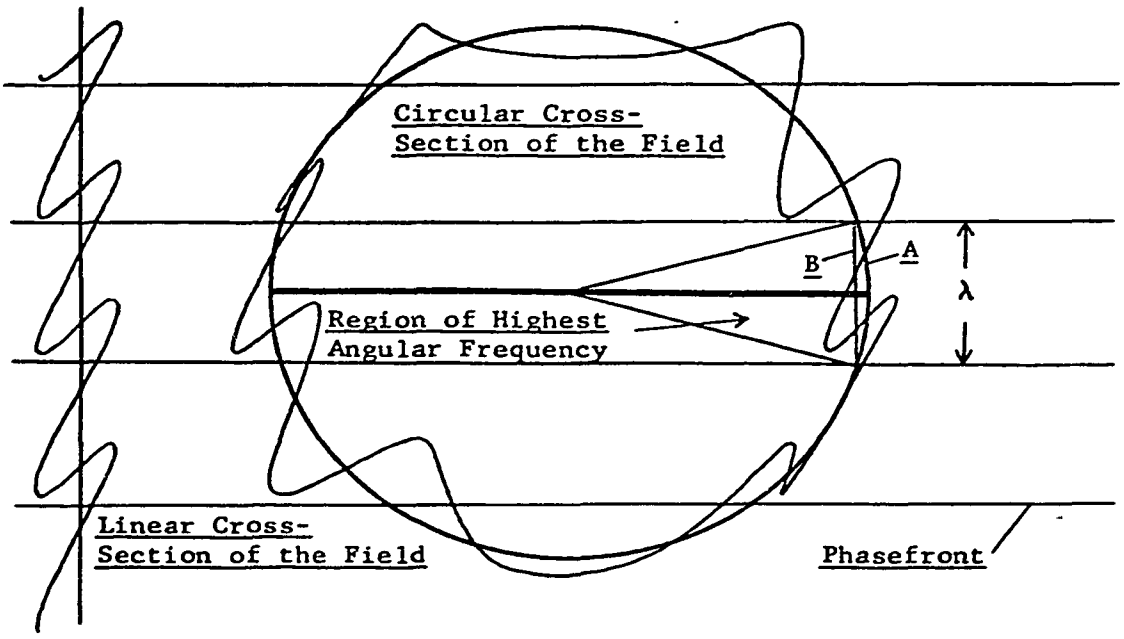

Figure 5.b.3 : If a cross-section of a plane wave field is made along a circular contour as shown in the diagram, the highest angular frequency occurs where the circle is intersected by the diameter parallel to the phasefronts. From this we can estimate the Fourier coefficient order necessary to reconstruct the cross-section.

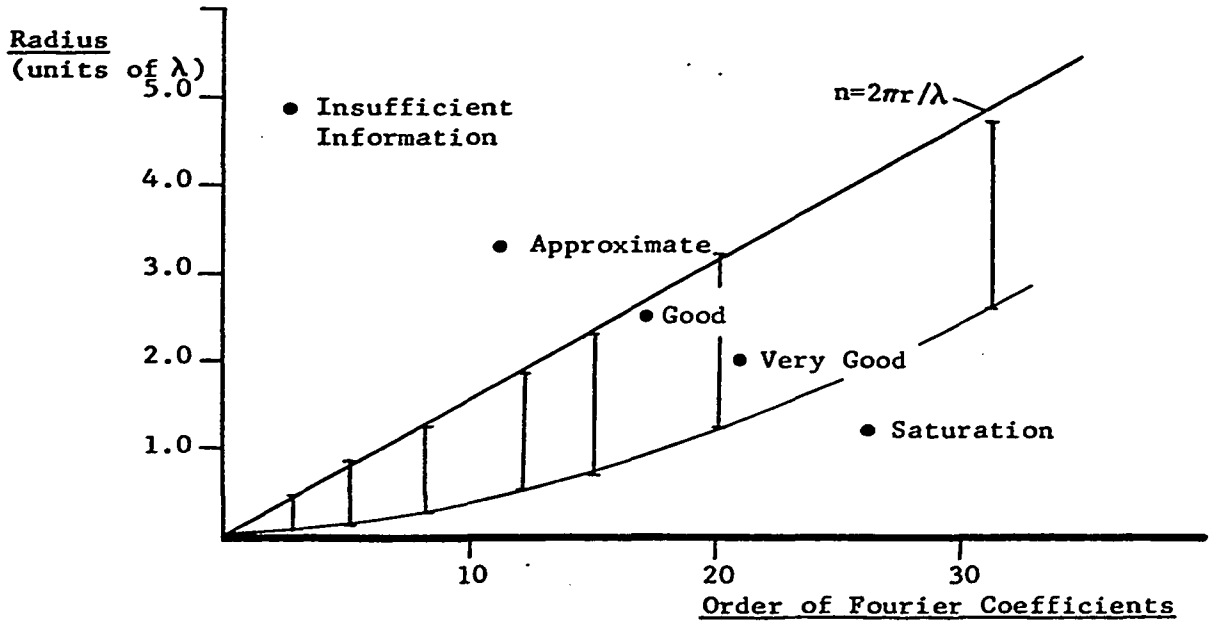

Figure 5.b.4 : Diagram showing the Fourier coefficient order necessary for good reconstruction at specific distances from the origin. The bounds are obtained primarily from the radial reconstructions of Section 5.e. The upper bound coincides with Equation 5.b.1.

5.c : Translations of the Pattern Function.

When the coordinate system is centered on the cylinder axis, the reconstructed field can accurately return the position of the conducting surface. If the coordinate system for the reconstruction is displaced from this axis, the accuracy decreases. Azimuthal reconstructions for very small translations appear nearly identical to their untranslated counterparts, but once the translation distance becomes more than a few percent of the cylinder radius a definite character governs the surface of minimum field. In Figure 5.c.1 a translation of ρ_o=0.28 for a 1.0λ radius cylinder shows a parabolic curve in the surface of minimum field. The surface should indicate minima at points near the cylinder. Strictly speaking, the analysis is not valid for reconstruction radii less than r=1.28 (the minimum radius enclosing the cylinder) but there is no saturation over the region shown in the diagram.

This raises the question of how much information is lost in translating a pattern function. In Figure 5.c.2 the order necessary to include all non-zero 5-6 decimal place Fourier coefficients is plotted against the minimum radius enclosing the cylinder for translated systems. Note that the untranslated cylinder requires 10 coefficients. These points form a slight upward curve which is well within the bounds determined in Section 5.b. The translation of Figure 5.c.1 fits right in this range, so the alteration in the shape of the returned conducting surface depends on degradations in the translated pattern function, and

not on an insufficient coefficient order. Similar conclusions can be drawn from Figures 5.c.3 and 5.c.4, where a 0.25λ radius cylinder has been translated with ρ_o=0.04.

While the information presented in Figures 5.c.2 and 5.c.4 is useful in determining a proper coefficient order for translated pattern functions, an analysis of the values generated by VARIA provides more information about the usefulness of the translated pattern functions themselves. Recall that VARIA preformed the operation described by Equation 2.2: a test of fit between a pattern function and a set of Fourier coefficients derived from it. Figure 5.c.5 shows the values of this subroutine plotted for many translation parameters of a 1.0λ radius cylinder. The Fourier coefficient order is 12. From Figure 5.c.2 we expect good results up to a minimum radius of r=1.2, or ρ_o=0.2. For 180° in Figure 5.c.5 this is exactly the case: the curve makes a sharp upward bend at this point. However, translations at angles other than ±180° and 0° causes sufficient asymmetry in the regenerated pattern function that the values of VARIA become orders of magnitude greater than those for translations along the incident direction. The mechanism for the translations themselves is tested by preforming double translations, out to a given point and back again, without calculating the new Fourier coefficients in the meantime. As we can see from the line of stars, they accurately return the value of VARIA for ρ_o=0. Therefore, the degeneration by translations from the preferred direction (the incident wave direction) is related to the

computing of the new Fourier coefficients. When the preferred direction is aligned with the pattern function symmetry axis (as in 180^{o} or 0^{o} translations) the regenerated coefficients match the pattern function. When translations at other angles are preformed, the pattern function symmetry is destroyed, and the test of Equation 2.2 indicates serious mismatching. For the data of Figure 5.c.1, VARIA returned a value of 36.45, a figure 9½ orders of magnitude above the figure for a centered coordinate system.

In Figure 5.c.6 some values returned by VARIA are plotted for translations involving three cylinder sizes. These are for optimal translations, with $\phi_o=180^{o}$. The 4.0λ radius cylinder shows mismatching due to the incomplete character of its pattern function (see Figure 3.3). The 1.0λ radius cylinder was discussed above. From Figure 5.c.4 we expect the curve for the 0.25λ radius cylinder (Fourier coefficient order 7) to turn upward near $\rho_o=0.05$, and it improves on our guess by remaining flat to $\rho_o=0.10$.

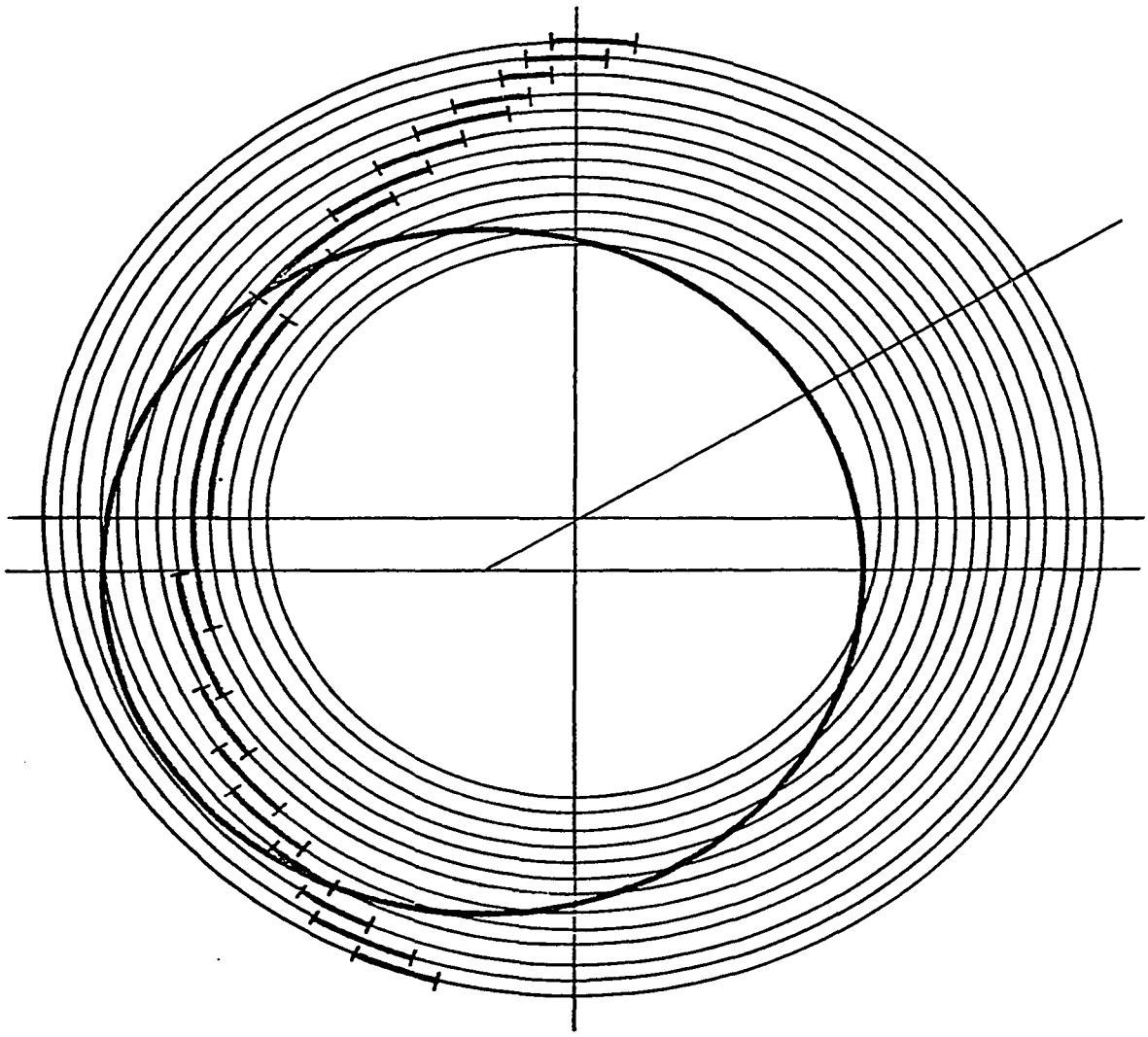

Figure 5.c.1 : Reconstruction in a coordinate system translated from the axis of a 1.0λ radius cylinder. ϕ_o=32° and ρ_o=0.28. The Fourier coefficient order is 15, and the radius varies from r=1.4 to r=0.8. Low points in the azimuthal scans are indicated by the heavy lines.

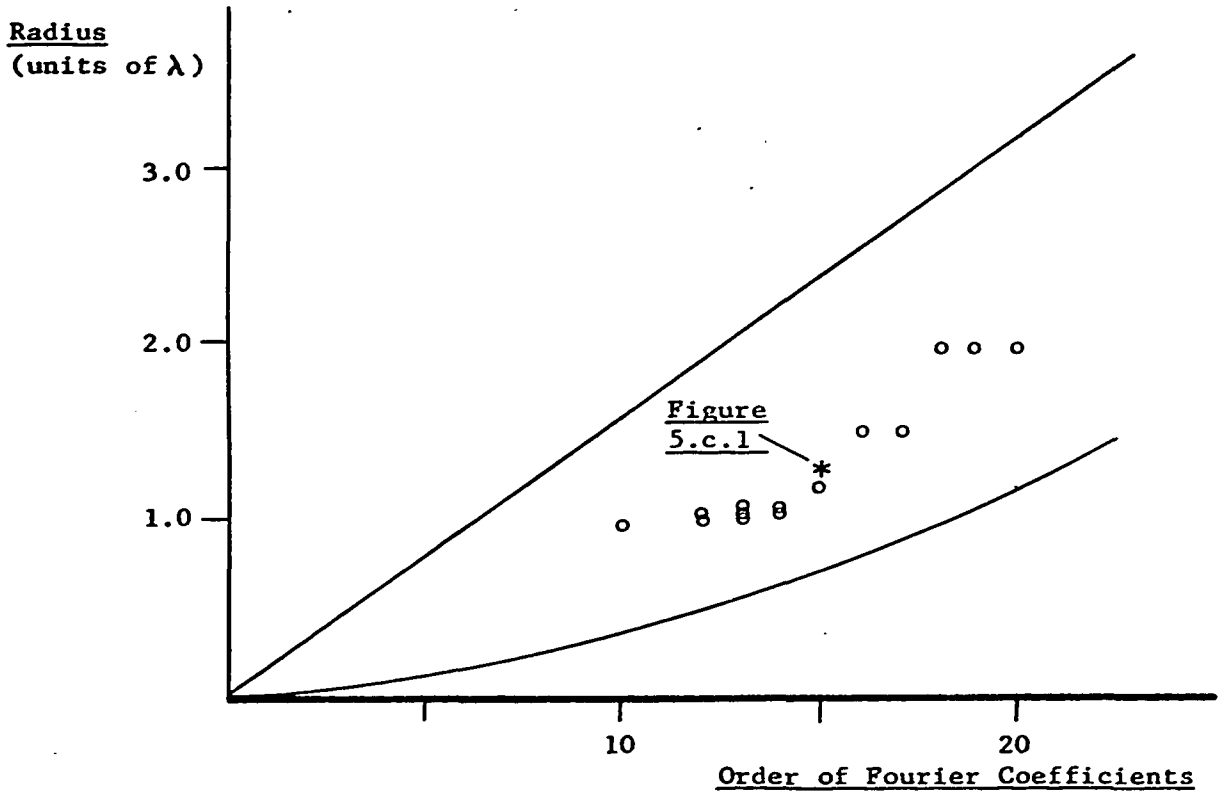

Figure 5.c.2 : Translations of a 1.0λ radius cylinder. Values of the minimum radius enclosing the cylinder vs. the Fourier coefficient order necessary to include all non-zero 5-6 decimal place coefficients are plotted with the bounds of Figure 5.b.4. The star indicates the position of the reconstruction in Figure 5.c.1.

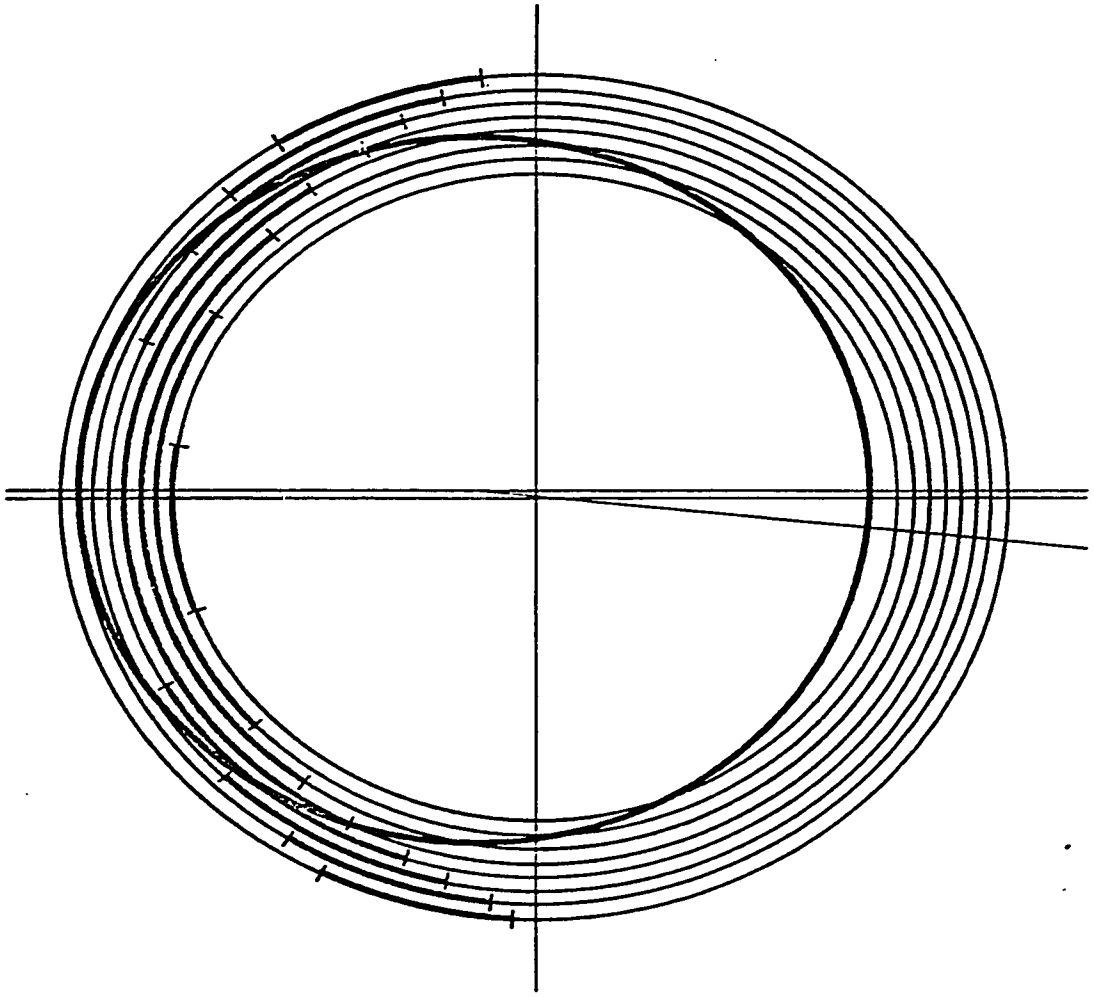

Figure 5.c.3 : Reconstruction in a coordinate system translated from the axis of a 0.25λ radius cylinder. ϕ_o=-6° and ρ_o=0.04. The Fourier coefficient order is 7, and the radius varies from r=0.30 to r=0.23. Low points in the azimuthal scans are indicated by the heavy lines.

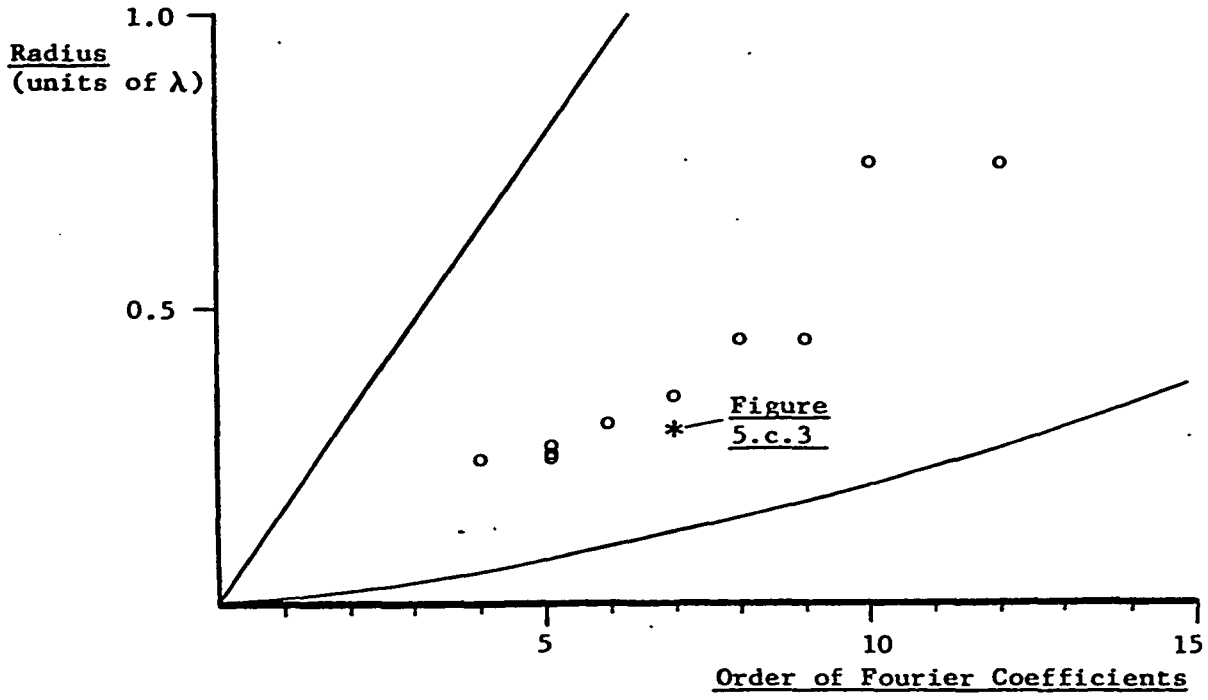

Figure 5.c.4 : Translations of a 0.25λ radius cylinder. Values of the minimum radius enclosing the cylinder vs. the Fourier coefficient order necessary to include all non-zero 5-6 decimal place coefficients are plotted with the bounds of Figure 5.b.4. The star indicates the position of the reconstruction in Figure 5.c.3.

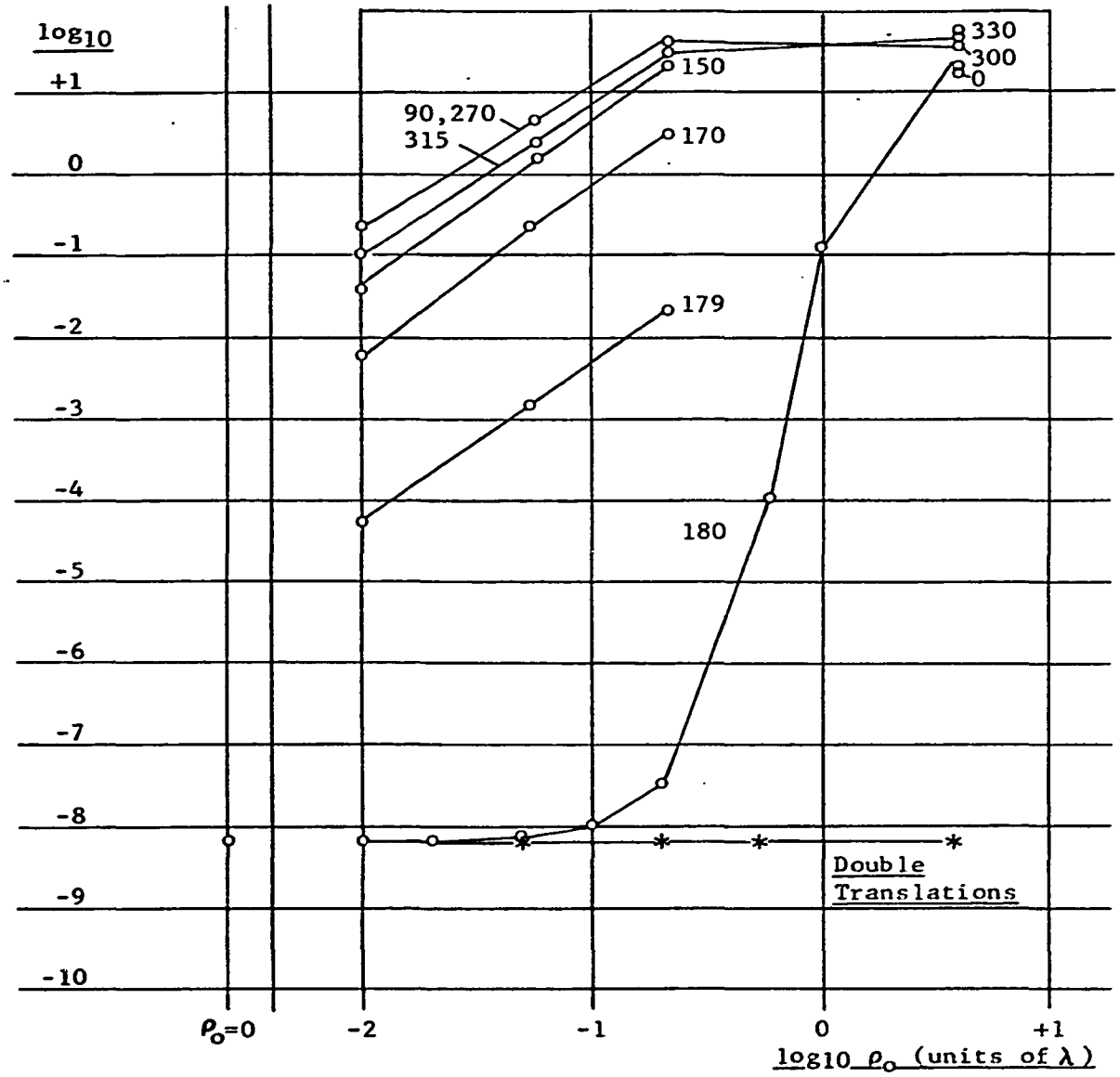

Figure 5.c.5 : Values returned by subroutine VARIA for translations of a 1.0λ radius cylinder. The Fourier coefficient order is 12. The angle ϕ_o is indicated in the diagram. Double translations (out from and back to the cylinder axis) are indicated by the stars.

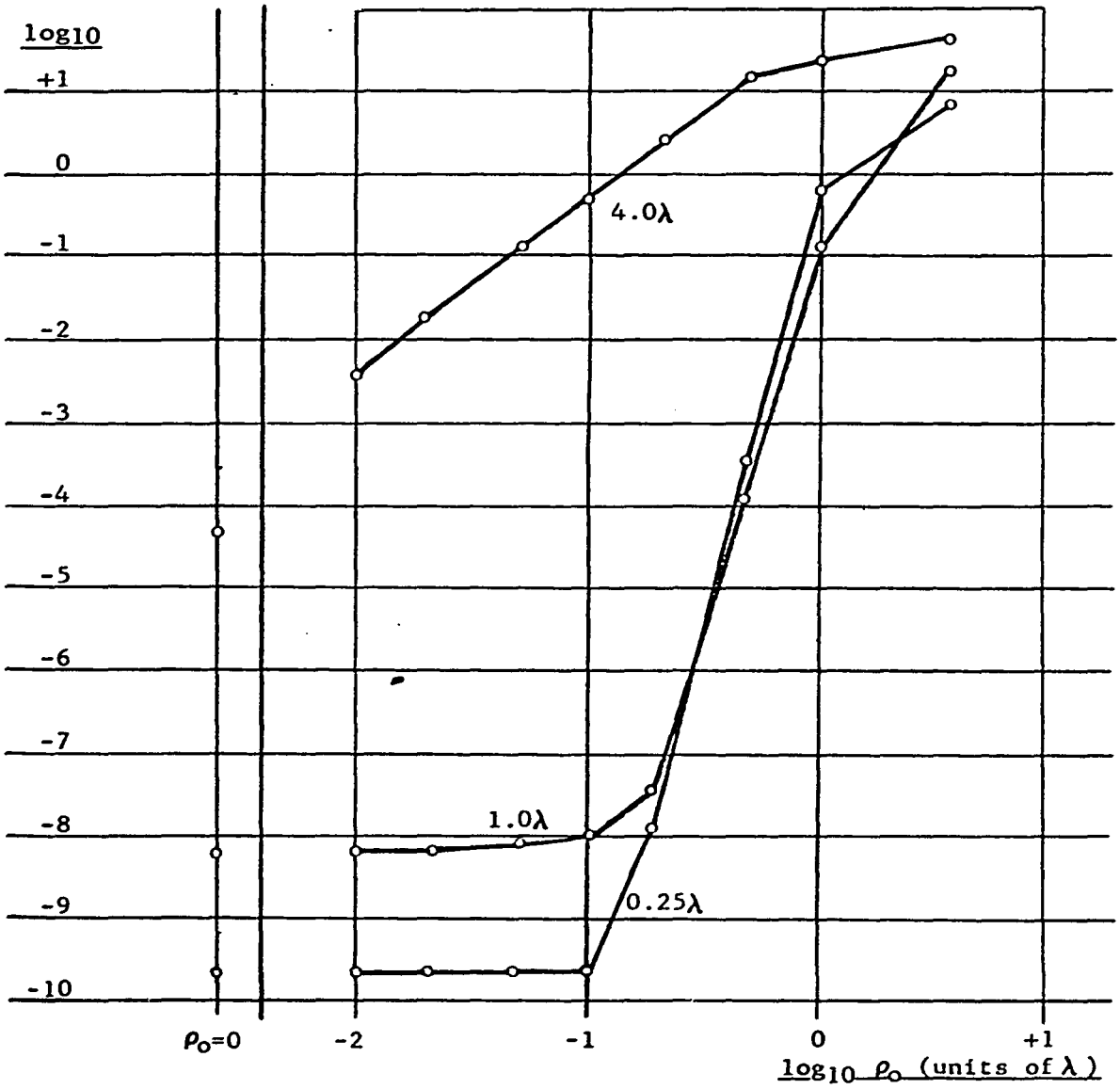

Figure 5.c.6 : Values returned by subroutine VARIA for translations of 0.25λ, 1.0λ, and 4.0λ radius cylinders. ϕ_o=180°. The Fourier coefficient order is 7 for the first case, 12 for the second, and 15 for the third. The pattern function data for the 4.0λ case is not constructed from all the non-zero 6 decimal place coefficients.

5.d : Reconstruction from Sectors of Pattern Data.

In Figures 5.d.1 and 5.d.2 we can see how the reconstruction process improves as larger angular sections of the pattern data are included in the analysis. Recall that 121 data points have been used to correspond to the 360° pattern function. We can see from the diagrams that even the removal of the two endpoints from the data set causes noticeable changes. In Figure 5.d.1 (r=1.5) the field for 354° (119 of the full 121 points) is only a bit more lumpy than the 360° case, but as the radius decreases, the fine structure dominates the pattern. Compare this with its counterpart in Figure 5.d.2 (r=1.2). The trend eventually reaches a limit at r=1.0 (not shown) when the fine structure begins to saturate the plotting space, in sharp contrast to the real field which we know is zero.

The removal of points from the data set causes the high order Fourier coefficients which are normally close to zero to be regenerated with large magnitudes. Essentially, they are trying to add a square well to the pattern function. Interpolation of the pattern data into the missing region would improve the reconstruction provided attention was paid to the aspects of information content discussed in Chapter 4. For the 1.0λ radius cylinder pattern data, interpolation should accurately re-establish data into missing regions extending to 90° since this size cylinder has four pair degrees of freedom. This figure might be considered an optimistic upper bound. However, when we observe the graph showing the real part of the true pattern function, Figure 5.d.3, it appears that a

quadratic scheme can easily fill missing points from -180° to -135° and from $+135^{\circ}$ to $+180^{\circ}$, a 90° extent. In this figure, the pattern is divided arbitrarily into four regions which seem to correspond to the output of four separate oscillators, and thereby to the conjectured four complex degrees of freedom. For non-interpolated sectors of pattern data, Figure 5.d.2 shows that we must accept information from better than 300° before reasonable judgments may be made about the reconstructed field close to the cylinder.

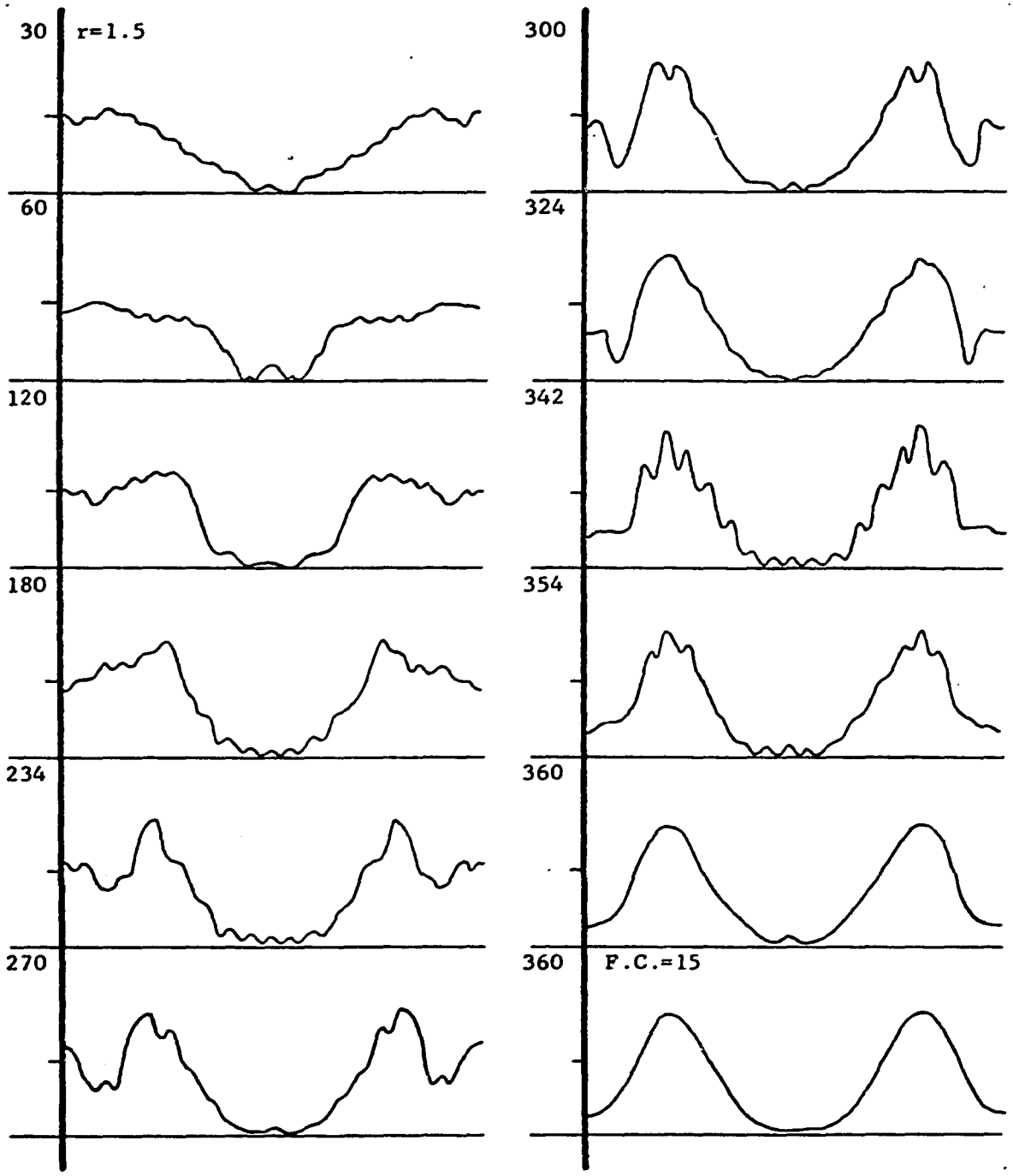

Figure 5.d.1 : Reconstruction with sectors of pattern function data (symmetrical about 0^{o}) for a 1.0λ radius cylinder. The Fourier coefficient order is 12 (15 in the lower 360^{o} diagram) and r=1.5.

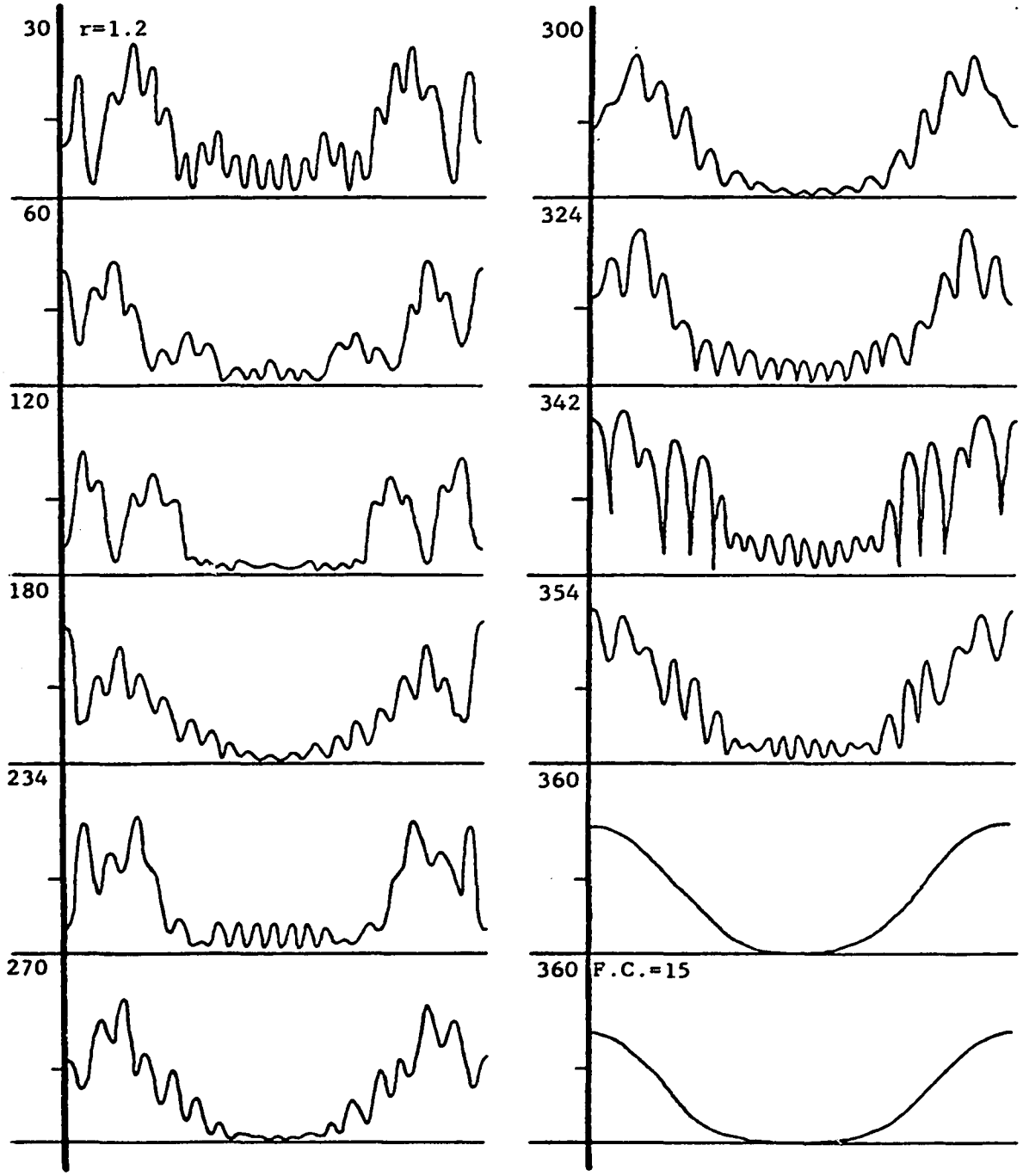

Figure 5.d.2 : Reconstruction with sectors of pattern function data (symmetrical about 0^{o}) for a 1.0λ radius cylinder. The Fourier coefficient order is 12 (15 in the lower 360^{o} diagram) and r=1.2.

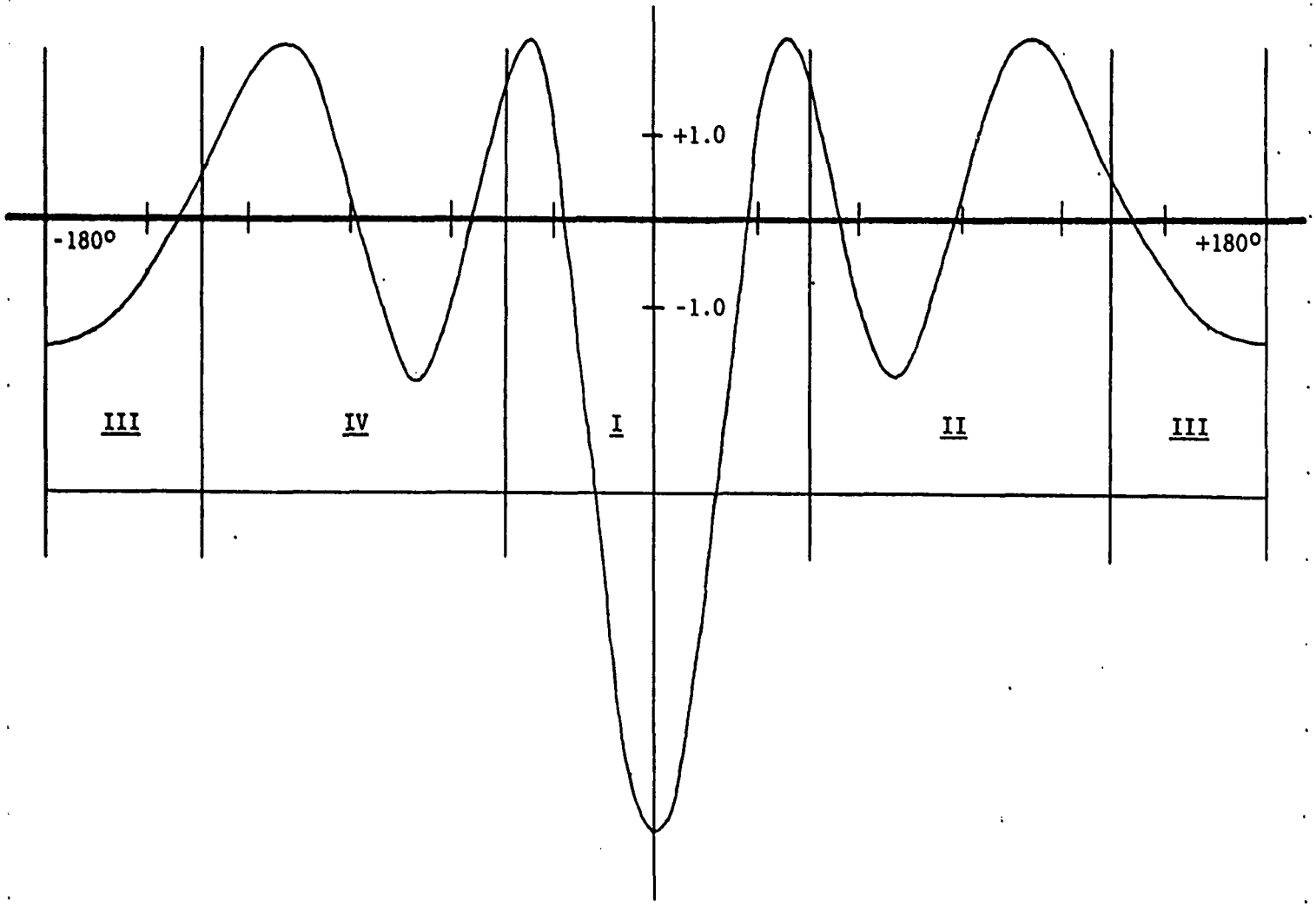

Figure 5.d.3 : Real part of the pattern function for a 1.0λ radius cylinder (ka=6.28). The pattern is divided into 90° sections corresponding to the four complex degrees of freedom of this scattering system.

5.e : Comparison with Experimental Data.

The final question we wish to raise in this study concerns the linking of the computational inverse scattering method to a real experiment. In fact, there is very good agreement between the reconstructed near field and an actual map of near-field values measured by Howarth (1971). In the experiment a 0.5" conducting cylinder was illuminated by a horn-fed microwave field with λ=12.75mm. Consequently, ka=3.16. The curvature of the incident field was about $1/6\lambda$ maximum over the region 5λ to one side of the cylinder, a fair plane wave approximation. The measured field was amplitude and phase referenced to the source, providing a map for each quantity. This data was then compared with the near field reconstructions for the ka=3.14 cylinder. Reconstructed values were plotted along two radial contours, at 300° and 330° (see Figure 5.e.1). Several different limits were used in the Fourier summations, and the regions of validity can be ascertained from the combined graphs in Figures 5.e.2 and 5.e.3. The circles indicate the field points taken from the map in Figure 5.e.1, and we see good matching along the 300° contour, and excellent matching at 330°.

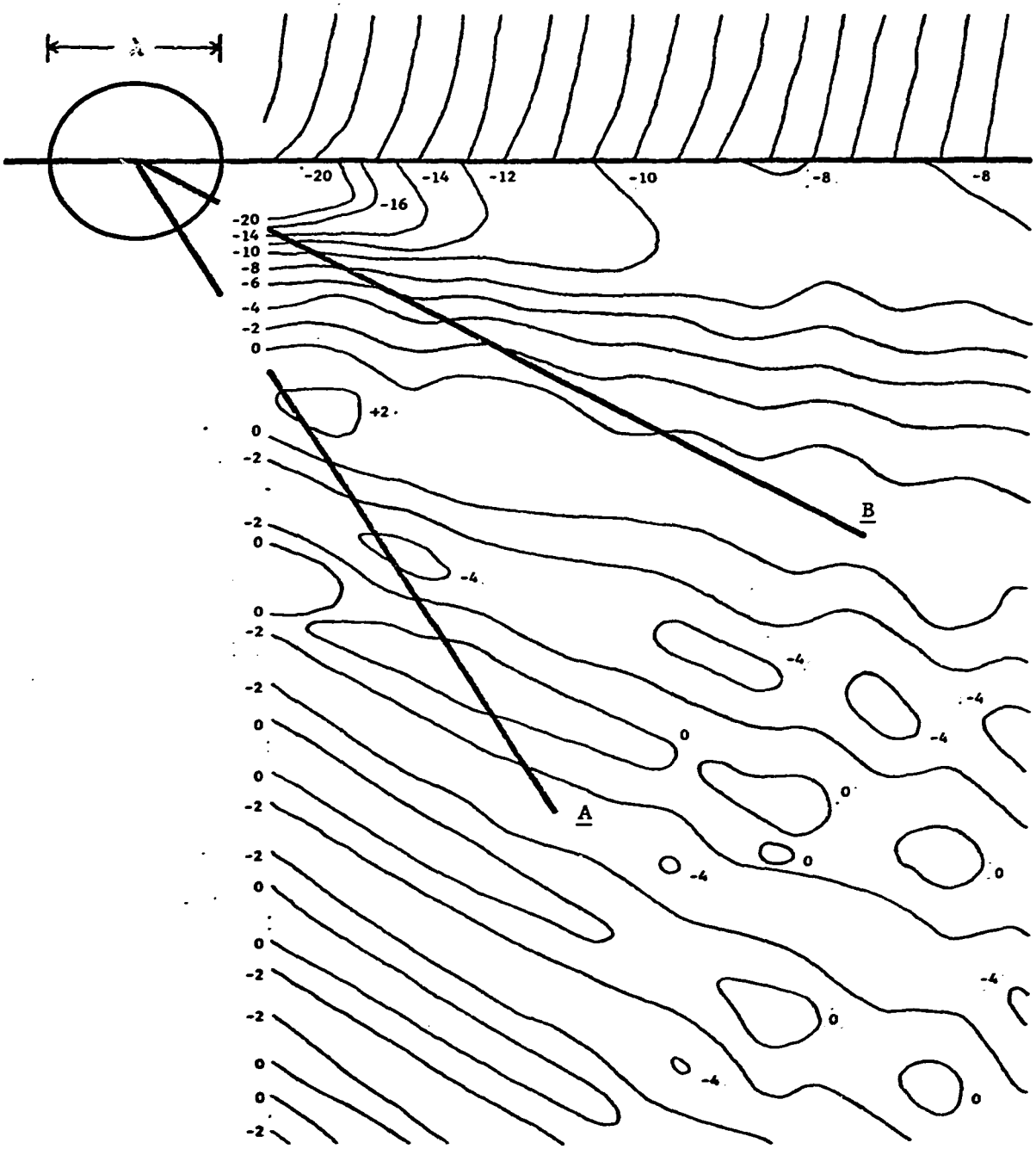

Figure 5.e.1 : Map of the field in the vicinity of a conducting cylinder illuminated by nearly plane waves (Howarth 1971). Ka=3.16, and the contours are scaled in db. A small section of the phase map appears at the top. The lines A and B refer to reconstructions found in Figures 5.e.2 and 5.e.3.

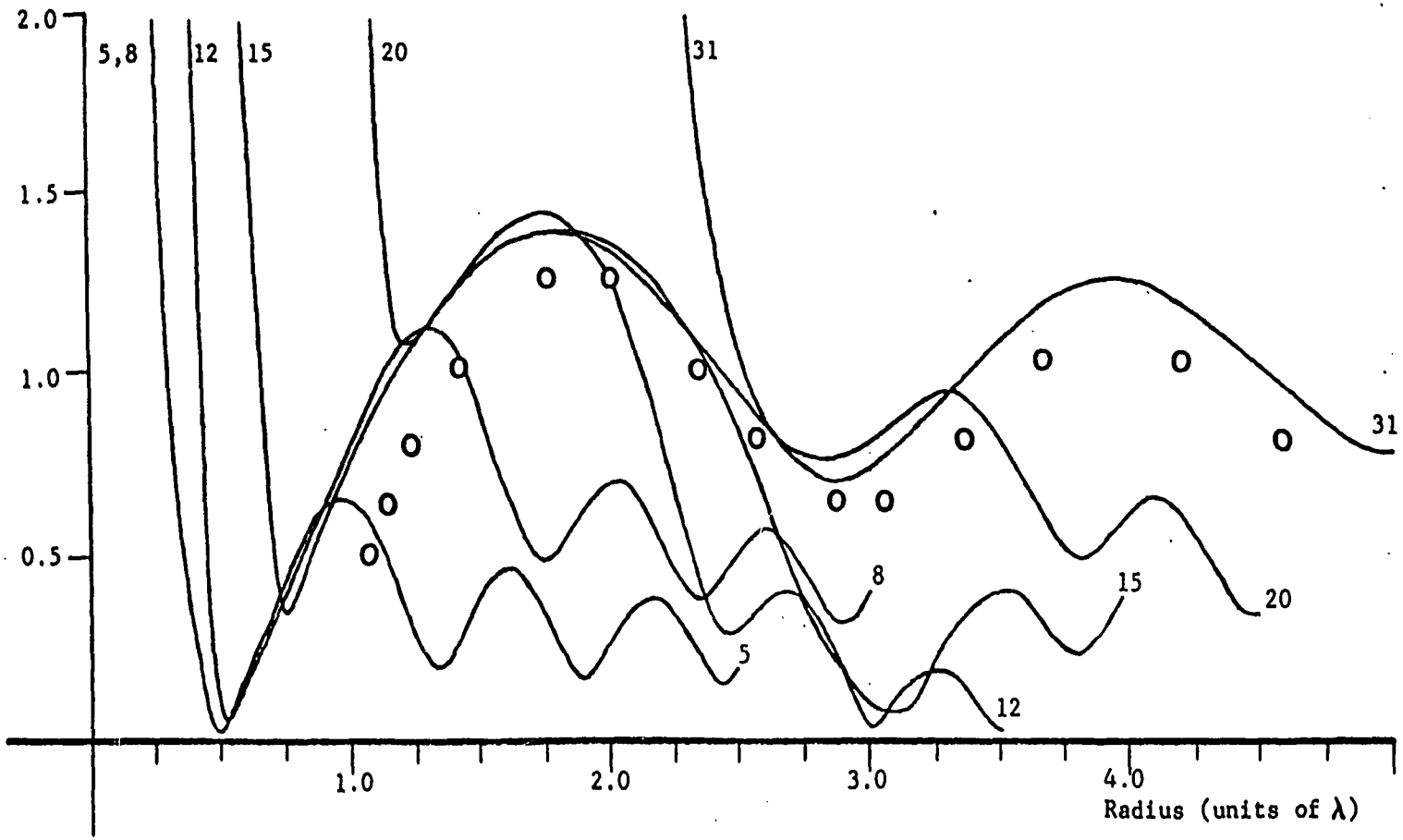

Figure 5.e.2 : Radial field reconstructions for the 0.5λ radius cylinder. Ka=3.14, the axis is at 300° (A in Figure 5.e.1), and the Fourier coefficient order is indicated in the diagram. The measured field for the ka=3.16 system is indicated by the circles.

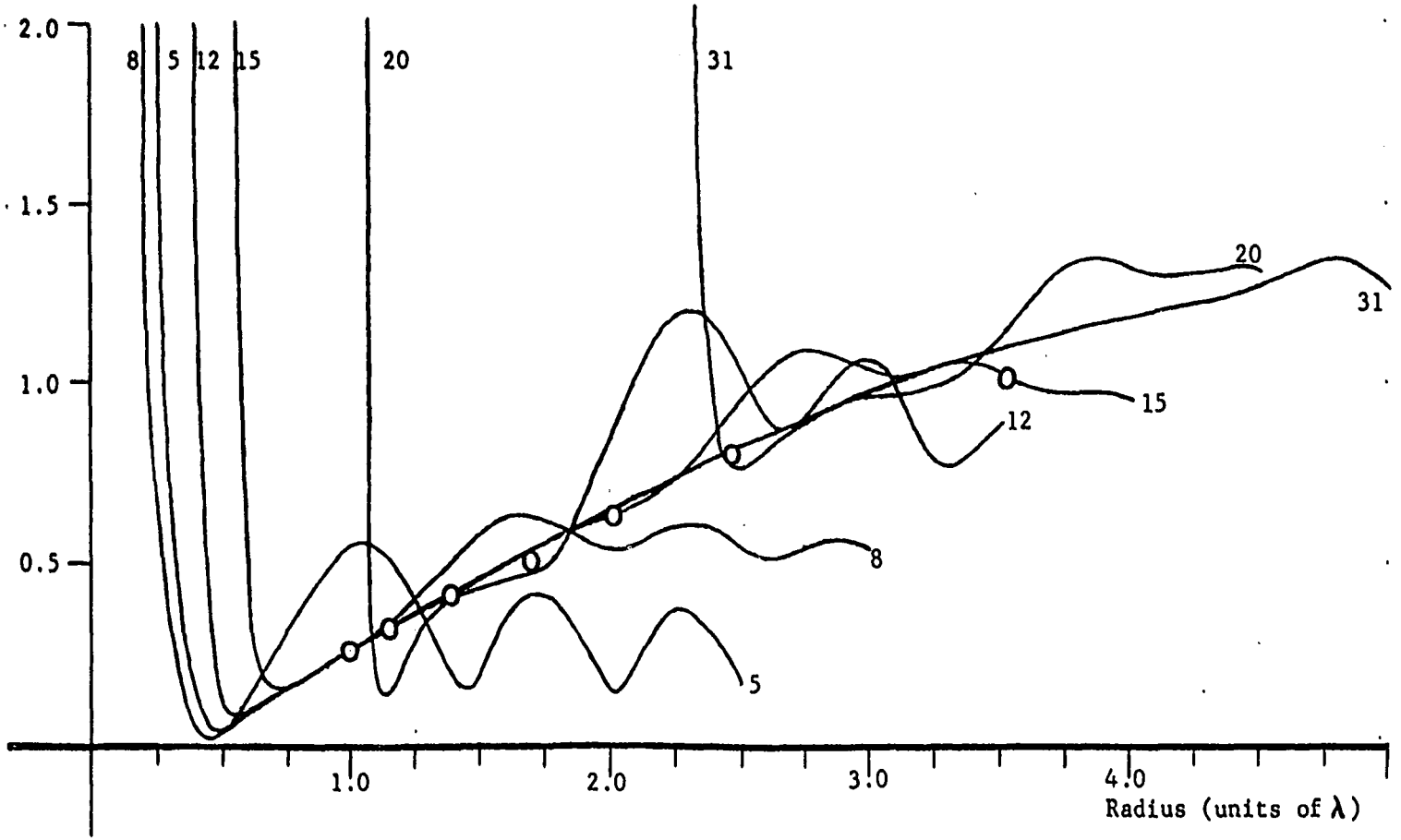

Figure 5.e.3 : Radial field reconstructions for the 0.5λ radius cylinder. Ka=3.14, the axis is at 330° (B in Figure 5.e.1), and the Fourier coefficient order is indicated in the diagram. The measured field for the ka=3.16 system is indicated by the circles.

CONCLUSION

In making a concise assessment of the Fourier analysis-Bessel function inverse scattering method, it can be said that it works, but that to work well, it requires precision that is not necessarily obtainable in practice. The technique definitely can be used in problems where the scatterer dimensions are in the order of a few wavelengths (which, of course, imposes a severe restriction on the recoverable detail), but it seems much too limited to handle the problem of distinguishing the B.A.C. 111 from the Boeing 727 in an air traffic control facility. A practical object recognition scheme will simply have to rely on much less scattered field data. Consequently, it will be wise to extend the application of the information content ideas in such a way that they will be able to show the effects of limited sampling. Also, work can be done with real-time correlation analysis, which has been a somewhat successful technique for providing information about colloids from the simultaneous measurement of scattered light intensity at a number of angles.

APPENDIX A1.

Inverse scattering program for azimuthal scans.
See Appendix A4 for a sample data module.

```
C     ------------------------------------------------------------------
C     INVERSC: THIS IS THE FORM OF THE INVERSE SCATTERING PROGRAM
C     DESIGNED TO RECONSTRUCT THE NEAR FIELD ALONG AZIMUTHAL CONTOURS.
C
C     SUBROUTINES NECESSARY: VARIA,HANK,TRANSG,EXPAND.
C
C     STRUCTURE OF THE DATA MODULE:
C        A.  PATTERN FUNCTION CARDS: 121 CARDS OF COMPLEX FAR FIELD
C            DATA, TABULATED IN 3 DEGREE INTERVALS FROM -PI TO +PI.
C            STATEMENT 01 FORMAT.
C        B.  INPUT CONTROL CARDS: STATEMENT 07 FORMAT. USE AS MANY AS
C            NECESSARY.
C        C.  0 CARD: 0 IN THE SECOND COLUMN.
C     ------------------------------------------------------------------
      IMPLICIT COMPLEX(A-G,O-Z)
      REAL LINE,LINEA
      DOUBLE PRECISION DPH,DPXA,DPYA,DPXB,DPYB
      DIMENSION GPHI(121),DPHI(121),H(63),DPXB(361),DPYB(361)
      DIMENSION LINE(51),LINEA(51),HIPHI(121)
      COMMON/DBLK/GPHI,NI,NF/ABLK/A(63)/DBLK/DPXA(361),DPYA(361),
     1DPXB,SPH,NSIM/GBLK/SPHI(361),NXI,NXF
      DATA BLANK,XAPOS,DOT,XTEN1,XTEN2,DAH/' ','H','.','HI','HL','H'/
      READ(5,01)GPHI
   01 FORMAT(10X,2F10.6)
      DO 30 I=1,121
   30 HIPHI(I)=GPHI(I)
      DPH=3.1415926536*3.0/180.0
      SPH=3.1415926536/180.0
      GO TO 062
   06 CONTINUE
      DO 061 I=1,121
  061 GPHI(I)=H(DPHI(I))
  062 CONTINUE
      READ(5,07)MD,NI,NF,NTH,XK,EPS,XA,XOFAC,DELTD,DMIN,XPOS,XNEG,XRFAC
   07 FORMAT(I2,3I3,2F10.6,7F5.2)
      IF(MD.EQ.0)GO TO 300
      WRITE(6,08)MD,NI,NF,XK,XA,NTH,XOFAC,XRFAC,DELTD,EPS,DMIN,XPOS,XNEG
   08 FORMAT('1','INPUT INFORMATION:',/,'0',' MD: DIMENSION OF THE FOURIE
     1R COEFFICIENT MATRIX: ',I2,/,' ','NI: START ANGLE (  1 = -PI): ',
     2I3,/,' ','NF: FINISH ANGLE (121 = +PI): ',I3,/,' ','XK: WAVENUMBER
     3: ',F10.6,/,' ','XA: CYLINDER RADIUS: ',F5.2,/,' ','NTH: INITIAL P
     4ATTERN TRANSLATION IN DEGREES: ',I4,/,' ','XOFAC: INITIAL PATTERN
     5TRANSLATION RADIUS FACTOR: ',F5.2,/,' ','XRFAC: INITIAL CLOSE-IN R
     6ADIUS FACTOR: ',F5.2,/,' ','DELTD: INITIAL CLOSE-IN STEP SIZE FACT.
     7OR: ',F5.2,/,' ','EPS: SURFACE TEST CUTOFF: ',F10.6,/,' ','DMIN: C
     8LOSE-IN STEP SIZE CUTOFF: ',F5.2,/,' ','XPOS: MAXIMUM CLOSE-IN RAD
     9IUS: ',F5.2,/,' ','XNEG: MINIMUM CLOSE-IN RADIUS: ',F5.2)
      DO 10 I=1,51
   10 LINEA(I)=BLANK
      DO 20 I=1,51,10
   20 LINEA(I)=DAH
      NXI=3*NI-2
      NXF=3*NF-2
      XRO=XOFAC*XA
      MC=(MD+1)/2
      XP1=0.0
      YP1=3.0
      XP2=0.0
      YP2=0.0
      MTHENTH
      MCOUNT=0
      IF(XTH.EQ.0.0)GO TO 03
   02 CALL TRANSG(NTH,XK,XRO)
      IF(NCOUNT.EQ.2)GO TO 021
      XP2=XP2+XRO*SIN(NTH*SPH)
      YP2=YP2+XRO*COS(NTH*SPH)
      GO TO 03
  021 XP2=XP2+XOFAC*XA*COS(MTH*SPH)+XRO*COS(NTH*SPH)
      YP2=YP2+XOFAC*XA*SIN(MTH*SPH)+XRO*SIN(NTH*SPH)
   03 CONTINUE
      CALL EXPAND
C     ------------------------------------------------------------------
C     GIVEN A PATTERN FUNCTION, THE FOURIER COEFFICIENTS UP TO A
C     DESIRED ORDER MA ARE COMPUTED.
C        MA=2*MA+1
C        NI=START ANGLE MEASURED IN INTEGRAL DEGREES EXPANDED BY 3.
C        NF=FINISH ANGLE MEASURED IN INTEGRAL DEGREES EXPANDED BY 3.
C     NORMALLY NI=1 AND NF=121,CORRESPONDING TO -PI AND +PI RESP.
C     ------------------------------------------------------------------
      DO 09 I=1,161
      DPXA(I)=0.0
   09 DPXB(I)=0.0
      DO 14 M=1,MD
      UT=FLOAT(M-MC)*SPH
      DO 12 N=NI,NXF
      UK=FLOAT(N-141)*UT
      UK=CMPLX(0.0,UK)
      USUM=GPXI(N)*CEXP(UK)
      DPXA(N)=DREAL(USUM)
      DPXB(N)=AIMAG(USUM)
   12 CONTINUE
      CALL DOSF(SPH,DPXA,DPYA,361)
      A(M)=SNGL(DPYA(NXF))/6.283185
      CALL DOSF(SPH,DPXB,DPYB,361)
      B=SNGL(DPYB(NXF))/6.283185
      A(M)=CMPLX(A(M),B)
   14 CONTINUE
      WRITE(6,15)
   15 FORMAT('1','RECONSTRUCTED FOURIER COEFFICIENTS')
      WRITE(6,16)(I,A(I),I=1,MD)
   16 FORMAT(' ',3X,I3,2X,2F10.6)
C     ------------------------------------------------------------------
C     FROM THE PATTERN FUNCTION GPHI WE HAVE COMPUTED A SET OF
C     FOURIER COEFFICIENTS A(I). WE WILL NOW RUN A TEST ON THESE
C     COEFFICIENTS TO SEE HOW WELL THEY RECONSTRUCT THE ORIGINAL
C     PATTERN FUNCTION.
C     ------------------------------------------------------------------
```

Al Continued.

```
      CALL VARIA(MR,VALUE)
      WRITE(6,10)VALUE
   10 FORMAT('0','TEST FIT VALUE ON INITIAL TRY=',F10.6)
      IF(NCOUNT.EQ.0)GO TO 91
      DO 92 I=1,121
   92 GPHI(I)=BPHI(I)
   91 CONTINUE
      NSUM=0
      XSUM=0.0
      YSUM=0.0
   94 UPDOWN=0.0
      DELTA=DELTO
      BAND=1.0
      ZERO=1.0
      XK=-RFAC*XK
      GJ=(0.0,1.0)
C     ---------------------------------------------------------------
C     AZIMUTHAL SCAN SECTION.                                       |
C     ---------------------------------------------------------------
   90 XKR=XK*XR
      IF(YR2.LE.0.005.AND.XR2.LE.0.005)GO TO 95
      RHO=SQRT(XR2**2+YR2**2)
      RTH=ATAN2(YR2,XR2)/SPH
      BK=-XK*RHO*COS(RTH-SPH)
      GF=CMPLX(0.0,BK)
      GO TO 96
   95 GF=(0.0,0.0)
   96 CONTINUE
      DO 100 N=1,ND
      ND=N-NC
      NM2=MOD(-ND,4)
      HX=HANK(XKR,ND)
      H(N)=A(N)*HX*GJ**NM2*CEXP(GF)*REAL(HX)*GJ**NM2
  100 CONTINUE
      DO 102 K=1,121
      DT=FLOAT(3*K-183)*SPH
      HSUM=(0.0,0.0)
      DO 101 JA=1,ND
      BK=FLOAT(JA-NC)*DT
      HK=CMPLX(0.0,BK)
      HSUM=HSUM+H(JA)*CEXP(HK)
  101 CONTINUE
      BPHI(K)=CABS(HSUM)
  102 CONTINUE
      WRITE(6,103)XR
  103 FORMAT('1','RADIUS IN CLOSE-IN SEQUENCE=',F7.4)
C     ---------------------------------------------------------------
C     PRINTER GRAPHING OF THE FIELD MAGNITUDE BPHI.                 |
C     ---------------------------------------------------------------
      DO 171 I=1,51
  171 LINE(I)=BLANK
      DO 172 I=1,121,2
      K=I+1
      WRITE(6,173)I,BPHI(I),K,BPHI(K),LINEA
  173 FORMAT(' ',3X,I3,2X,F10.6,5X,I3,2X,F10.6,12X,51A1)
      IX=IFIX(20.0*BPHI(I)+1.5)
      IF(IX.LT.1)GO TO 174
      IF(IX.GT.51)GO TO 175
      LINE(IX)=XAPUS
      GO TO 176
  175 IX=51
      LINE(IX)=XTEN1
  176 WRITE(6,177)LINE
  177 FORMAT('+',50X,51A1)
      LINE(IX)=BLANK
  174 KK=IFIX(20.0*BPHI(K)+1.5)
      IF(KK.LT.1)GO TO 172
      IF(KK.GT.51)GO TO 178
      LINE(KK)=DOT
      GO TO 179
  178 KK=51
      LINE(KK)=XTEN2
  179 WRITE(6,180)LINE
  180 FORMAT('+',50X,51A1)
      LINE(KK)=BLANK
  172 CONTINUE
      NZERO=0
      DO 120 K=1,121
      IF(BPHI(K).GT.EPS)GO TO 120
      X=XR1+XR*COS(FLOAT(3*K-183)*SPH)
      Y=YR1+XR*SIN(FLOAT(3*K-183)*SPH)
      XSUM=XSUM+X
      YSUM=YSUM+Y
      NSUM=NSUM+1
      WRITE(6,118)
  118 FORMAT('0','    X          Y          BPHI')
      WRITE(5,119)X,Y,BPHI(K)
  119 FORMAT(' ',3F10.6)
      NZERO=1
  120 CONTINUE
C     ---------------------------------------------------------------
C     THE FOLLOWING SEQUENCE PROVIDES A METHOD OF CLOSING IN ON THE |
C     CIRCLE JUST CONTAINING THE CONDUCTING SURFACE. THE CUTOFF IS  |
C     CHOSEN TO PROVIDE AN ACCURACY OF DMIN*DELTA.                  |
C     ---------------------------------------------------------------
      IF(UPDOWN.EQ.0.0)GO TO 204
      IF(UPDOWN.EQ.-1.0)GO TO 202
      IF(NZERO.EQ.1)GO TO 201
      BAND=0.5
      ZERO=-1.0
      GO TO 207
  201 ZERO=1.0
      GO TO 207
  202 IF(NZERO.EQ.1)GO TO 203
      ZERO=-1.0
      GO TO 207
  203 BAND=0.5
      ZERO=1.0
```

A1 Continued.

```
      GO TO 207
  204 IF(NZERO.EQ.1)GO TO 205
      UPDOWN=-1.0
      GO TO 206
  205 UPDOWN=1.0
  206 DELTA=ABS(DELTA)*UPDOWN
      GO TO 208
  207 DELTA=ABS(DELTA)*BAND*ZERO
      IF(ABS(DELTA).LT.DMIN)GO TO 210
  208 XR=XR+DELTA*XA
      IF(XR.GT.X305.OR.XR.LT.XNEG)GO TO 209
      GO TO 99
  210 NCOUNT=NCOUNT+1
      IF(NCOUNT.EQ.1)GO TO 211
      IF(NCOUNT.EQ.2)GO TO 212
      GO TO 299
  211 XAV=XSUM/FLOAT(NSUM)
      YAV=YSUM/FLOAT(NSUM)
      X01=XAV
      Y01=YAV
      R00=SQRT(XAV**2+YAV**2)
      NTH=IFIX(ATAN2(YAV,XAV)/SPH)
      DO 213 I=1,121
  213 GPHI(I)=GPHI(I)
      GO TO 02
  212 XAV=XSUM/FLOAT(NSUM)
      YAV=YSUM/FLOAT(NSUM)
      X1=(XAV+2.0*X01)/2.0
      Y1=(YAV+2.0*Y01)/2.0
      R00=SQRT(X1**2+Y1**2)
      NTH=IFIX(ATAN2(Y1,X1)/SPH)
      GO TO 02
  299 CONTINUE
      GO TO 06
  300 CONTINUE
      STOP
      END
```

APPENDIX A2.

Inverse scattering program for radial scans.
See Appendix A4 for a sample data module.

```
C     ------------------------------------------------------------------
C     INVERSE: THIS IS THE FORM OF THE INVERSE SCATTERING PROGRAM
C     DESIGNED TO RECONSTRUCT THE NEAR FIELD ALONG RADIAL CONTOURS.
C     ------------------------------------------------------------------
C     SUBROUTINES NECESSARY: VARIA,HANK,TRANSG,EXPAND.
C
C     CARE MUST BE TAKEN IN BUILDING THE DATA MODULE:
C        A.  PATTERN FUNCTION CARDS: 121 CARDS OF COMPLEX FAR FIELD
C            DATA, TABULATED IN 3 DEGREE INTERVALS FROM -PI TO +PI.
C            STATEMENT 01 FORMAT.
C        B.  SETUP CARD: STATEMENT 06 FORMAT.
C        C.  RADIAL SCAN CARD: STATEMENT 31 FORMAT. USE AS MANY RADIAL
C            SCANS AS NECESSARY FOR EACH SETUP CARD.
C        D.  T CARD: T IN COLUMN 1.
C        E.  0 CARD: 0 IN COLUMN 2.
C     THE GROUP (B,C,D) MAY BE REPEATED BEFORE THE E CARD.
C     ------------------------------------------------------------------
      IMPLICIT COMPLEX(A,G,H)
      REAL LINE,LINEA
      DOUBLE PRECISION DPH,DPXA,DPYA,DPXH,DPYH
      DIMENSION H1(63),H2(63),DPXH(361),DPYH(361)
      DIMENSION LINE(51),LINEA(51),GIPHI(121)
      COMMON/GBLK/GPHI(121),NI,NF/AHLK/A(63)/DBLK/DPXA(361),DPYA(361),
     1DPH,SPH,NDIM/GXBLK/GPXI(361),NXI,NXF
      DATA BLANK,XAP05,DOT,XTEN1,XTEN2,BAR/1H ,1H*,1H.,1HT,1HL,1H|/
      READ(5,01)SPHI
   01 FORMAT(10X,2F10.6)
      DO 02 I=1,121
   02 GIPHI(I)=GPHI(I)
      DPH=3.14159265358*3.0/180.0
      SPH=3.14159265358/180.0
      GO TO 05
   03 CONTINUE
      DO 04 I=1,121
   04 GPHI(I)=GIPHI(I)
   05 CONTINUE
      READ(5,06)MH,NI,NF,NTH,XK,XDFAC,XA
   06 FORMAT(I2,3I3,2F10.6,F5.2)
      IF(MH.EQ.0)GO TO 100
      WRITE(6,07)MH,NI,NF,NTH,XK,XA,XDFAC
   07 FORMAT('1','SETUP INFORMATION:',/,'0',8X,I2,2X,'MH: DIMENSION OF T
     1HE FOURIER COEFFICIENT MATRIX',/,' ',7X,I3,2X,'NI: START ANGLE  (
     2  I=-PI)',/,' ',7X,I3,2X,'NF: FINISH ANGLE (121=+PI) ',/,' ',7X,I3
     3,2X,'NTH: INITIAL PATTERN TRANSLATION IN DEGREES.',/,' ',F10.6,2X,
     4'XK: WAVENUMBER.',/,' ',F10.6,2X,'XA: RADIAL UNIT DISTANCE.',/,' '
     5,F10.6,2X,'XDFAC: INITIAL PATTERN TRANSLATION RADIUS FACTOR.')
      DO 08 I=1,51
   08 LINEA(I)=BLANK
      DO 09 I=1,51,10
   09 LINEA(I)=BAR
      NXI=3*NI-2
```

A2 Continued.

```
      NRF=3*NF-2
      XRO=XOFAC*XA
      MTH=NTH
      XMFAC=XOFAC
      MC=(MM+1)/2
      IF(XRO.EQ.0.0)GO TO 12
   10 CALL TRANSG(NTH,XK,XRO)
C     ------------------------------------------------------------------
C     GIVEN A PATTERN FUNCTION, THE FOURIER COEFFICIENTS UP TO A       |
C     DESIRED ORDER MA ARE COMPUTED.                                   |
C        MM=2*MA+1                                                     |
C        NI=START ANGLE MEASURED IN INTEGRAL DEGREES EXPANDED BY 3.    |
C        NF=FINISH ANGLE MEASURED IN INTEGRAL DEGREES EXPANDED BY 3.   |
C     NORMALLY NI=1 AND NF=121,CORRESPONDING TO -PI AND +PI RESP.      |
C     ------------------------------------------------------------------
   12 CALL FSPAN
      DO 15 I=1,361
      DPXA(I)=0.0
   15 DPXB(I)=0.0
      DO 17 M=1,MM
      RT=FLOAT(M-MC)*SPH
      DO 16 N=NI,NRF
      RK=FLOAT(N-181)*RT
      HK=CMPLX(0.0,RK)
      HSUM=GPX1(N)*CEXP(HK)
      DPXA(N)=REAL(HSUM)
      DPXB(N)=AIMAG(HSUM)
   16 CONTINUE
      CALL DQSF(3PH,DPXA,DPYA,361)
      FI=SNGL(DPYA(NRF))/6.283185
      CALL DQSF(3PH,DPXB,DPYB,361)
      F2=SNGL(DPYB(NRF))/6.283185
      A(M)=CMPLX(FI,F2)
   17 CONTINUE
      WRITE(6,18)
   18 FORMAT('1','RECONSTRUCTED FOURIER COEFFICIENTS.')
      WRITE(6,19)(I,A(I),I=1,MM)
   19 FORMAT(' ',3X,I3,2X,2F10.6)
C     ------------------------------------------------------------------
C     FROM THE PATTERN FUNCTION GPH1 WE HAVE COMPUTED A SET OF         |
C     FOURIER COEFFICIENTS A(MM). WE WILL NOW RUN A TEST ON THESE      |
C     COEFFICIENTS TO SEE HOW WELL THEY RECONSTRUCT THE ORIGINAL       |
C     PATTERN FUNCTION.                                                |
C     ------------------------------------------------------------------
      CALL VARIA(MM,VALUE)
      WRITE(6,20)VALUE
   20 FORMAT('0','TEST FIT TO PATTERN FUNCTION =',F10.6)
      XOI=XOFAC*XA*COS(NTH*SPH)
      YOI=XOFAC*XA*SIN(NTH*SPH)
C     ------------------------------------------------------------------
C     RADIAL SCAN SECTION.                                             |
C     ------------------------------------------------------------------
   30 READ(5,31)TRACKA,RMIN,RMAX,XANGLE,SCALE
   31 FORMAT(A1,1X,4F10.6,F10.4)
      IF(TRACKA.EQ.XTEN)GO TO 03
      WRITE(6,32)RMIN,RMAX,XANGLE,SCALE
   32 FORMAT('1','RADIAL SCAN.',8X,'RMIN:',F10.6,'    RMAX:',F10.6,
     1'    XANGLE (DEGREES):',F10.6,'    POINTS PER UNIT RADIUS:',F10.4)
      DO 33 I=1,91
   33 LINE(I)=BLANK
      PI=RMIN
      R2=RMIN+1.0/SCALE
      FC=XA*COS(XANGLE*SPH)
      FS=XA*SIN(XANGLE*SPH)
   40 X1=XOI+R1*FC
      X2=XOI+R2*FC
      Y1=YOI+R2*FS
      Y2=YOI+R2*FS
      RNEW1=SQRT(X1**2+Y1**2)
      RNEW2=SQRT(X2**2+Y2**2)
      XANG1=ATAN2(Y1,X1)/SPH
      XANG2=ATAN2(Y2,X2)/SPH
      GJ=(0.0,1.0)
      XKR1=XK*R1
      XKR2=XK*R2
      DO 41 N=1,MM
      ND=N-MC
      NM2=MOD(-ND,4)
      GF=GJ**NM2
      HX1=HANK(XKR1,ND)
      HX2=HANK(XKR2,ND)
      BT1=-XK*RNEW1*SPH*COS(XANG1*SPH)
      BT2=-XK*RNEW2*SPH*COS(XANG2*SPH)
      HK1=CMPLX(0.0,BT1)
      HK2=CMPLX(0.0,BT2)
      H1(N)=A(N)*HX1*GF*CEXP(HK1)*REAL(HX1)*GF
      H2(N)=A(N)*HX2*GF*CEXP(HK2)*REAL(HX2)*GF
   41 CONTINUE
      BT=XANGLE*SPH
      HSUM1=(0.0,0.0)
      HSUM2=(0.0,0.0)
      DO 42 JA=1,MM
      RK=FLOAT(JA-MC)*BT
      HK=CMPLX(0.0,RK)
      HSUM1=HSUM1+H1(JA)*CEXP(HK)
      HSUM2=HSUM2+H2(JA)*CEXP(HK)
   42 CONTINUE
      BPHI1=CABS(HSUM1)
      BPHI2=CABS(HSUM2)
C     ------------------------------------------------------------------
C     PRINTER GRAPHING OF THE FIELD MAGNITUDE BPHI.                    |
C     ------------------------------------------------------------------
      WRITE(6,50)PI,BPHI1,R2,BPHI2,LINEA
   50 FORMAT(' ',3X,F6.3,2X,F10.6,5X,F6.3,2X,F10.6,11X,91A1)
      IX=IFIX(20.0*BPHI1+1.5)
      IF(IX.LT.1)GO TO 54
```

A2 Continued.

```
      IF(IX.GT.51)GO TO 51
      LINE(IX)=XAPOS
      GO TO 52
   51 IX=51
      LINE(IX)=XTPNT
   52 WRITE(6,53)LINE
   53 FORMAT(' ',55X,51A1)
      LINE(IX)=BLANK
   54 XX=IFIX(20.0*DPHI2+1.5)
      IF(XX.LT.1)GO TO 56
      IF(XX.GT.51)GO TO 55
      LINE(XX)=DOT
      GO TO 56
   55 XX=51
      LINE(XX)=XTPNT2
   56 WRITE(6,57)LINE
   57 FORMAT(' ',55X,51A1)
      LINE(XX)=BLANK
   58 CONTINUE
      R1=R1*2.0/SCALE
      R2=R2*2.0/SCALE
      IF(N1.GT.NMAX)GO TO 30
      GO TO 40
  100 CONTINUE
      STOP
      END
```

APPENDIX A3.

Subroutines and functions.

```
      SUBROUTINE TRANSG(NTH,XK,XR0)
C     ------------------------------------------------------------------
C     THIS SUBROUTINE REGENERATES THE PATTERN FUNCTION FOR A            |
C     TRANSLATION OF THE COORDINATE AXES. XR0 IS THE RADIUS BETWEEN     |
C     THE ORIGINS, AND NTH IS THE INTEGRAL NUMBER OF DEGREES IN THE     |
C     ANGULAR SEPARATION FROM THE ORIGINAL TO THE NEW ORIGIN. XK IS THE  |
C     WAVENUMBER.                                                       |
C     ------------------------------------------------------------------
      IMPLICIT COMPLEX (G)
      COMMON/GBLK/GPHI(121),NI,NF
      SPH=3.14159265358/180.0
      DO 01 I=NI,NF
      MM=I-181-NTH
      IF(MM.LT.-180)MM=MM+360
      BT=SPH*FLOAT(MM)
      RK=XK*XR0*COS(BT)
      GK=CMPLX(0.0,RK)
   01 GPHI(I)=GPHI(I)*CEXP(GK)
      WRITE(6,02)NTH,XK,XR0
   02 FORMAT('1','TRANSLATION OF THE PATTERN FUNCTION.',/,'0','NTH:  XK:
     1       XR0:',/,' ',I4,1X,2F10.6,/,'0','TRANSLATED GPHI.')
      DO 04 I=1,41
      I41=I+41
      I82=I+82
      WRITE(6,03)I,GPHI(I),I41,GPHI(I41),I82,GPHI(I82)
   03 FORMAT(' ',3X,I1,2X,2F10.6,17X,I3,2X,2F10.6,17X,I3,2X,2F10.6)
   04 CONTINUE
      RETURN
      END
```

```
      COMPLEX FUNCTION HANK(R,M)
C     ------------------------------------------------------------------
C     THIS COMPLEX FUNCTION COMPUTES A HANKEL FUNCTION OF THE 2ND KIND.  |
C     ------------------------------------------------------------------
      DIMENSION WORD(2)
      COMPLEX TEMP1,TEMP2
      COMMON /OPRR/K1,K2,IRR1(5),IRR2(5),ERAN(2,5),ERHN(2,5)
      DATA WORD(1),WORD(2)/4HBESJ,4HBESY/,PI/3.141593/
C
      N=IABS(M)
      IF(R.GE.10.0.AND.R.GT.FLOAT(N)) GO TO 1
      CALL BESJ(R,N,BJA,0.0005,IER)
      IF(IER.GT.0) GO TO 10
    4 CALL BESY(R,N,BYA,IER)
      IF(IER.GT.0) GO TO 15
      HANK=CMPLX(BJA,-BYA)
    3 IF(M.GE.0) RETURN
      IF(MOD(N,2).GT.0) HANK=-HANK
      RETURN
C
```

A) Continued.

```
    1 NI=N
      IF(N.GT.5) NI=6
      SQR=SQRT(2.0/(PI*R))
      CHI=R-(FLOAT(NI)+0.5)*PI/2.0
      U=4.0*FLOAT(NI)**2)
      Z=2.0*(8.0*R)**2
      P=1.0
      IF(N.GT.5) P=1.0-(U-169.0)*(U-225.0)/(28.0*Z)
      IF(N.GE.4) P=1.0-P*(U-81.0)*(U-121.0)/(15.0*Z)
      P=1.0-P*(U-25.0)*(U-49.0)/(6.0*Z)
      P=1.0-P*(U-1.0)*(U-9.0)/Z
      Q=1.0
      IF(N.GE.5) Q=1.0-(U-121.0)*(U-169.0)/(21.0*Z)
      IF(N.GE.3) Q=1.0-Q*(U-49.0)*(U-81.0)/(10.0*Z)
      Q=1.0-Q*(U-9.0)*(U-25.0)/(3.0*Z)
      Q=Q*(U-1.0)/(8.0*R)
      HANK=SQR*CMPLX(P,-Q)*CMPLX(COS(CHI),-SIN(CHI))
      IF(NI.EQ.N) GO TO 3
      CHI=R-2.75*PI
      P=1.0-(9009.0/Z)*(1.0-(637.5/Z)*(1.0+(26.6/Z)*(1.0-308.03571/Z)))
      Q=(12.375/R)*(1.0-(2275.0/Z)*(1.0-(96.9/Z)*(1.0-69.0/Z)))
      TEMP2=SQR*CMPLX(P,-Q)*CMPLX(COS(CHI),-SIN(CHI))
    2 TEMP1=HANK
      HANK=2.0*FLOAT(NI)*TEMP1/R-TEMP2
      NI=NI+1
      IF(NI.GT.N) GO TO 3
      TEMP2=TEMP1
      GO TO 2
C
   10 IF(IER.NE.3) GO TO 11
      K2=K2+1
      IF(K2.LT.1.OR.K2.GT.5) GO TO 4
      ENUM(1,K2)=R
      IND2(K2)=N
      ENUM(2,K2)=BJA
      GO TO 4
   11 PRINT 12,WORD(1),IER,R,N,WORD(1),BJA,
   12 FORMAT(35H0--- FUNCTION 'HANK' - SUBROUTINE ',1A4,
     121H' - ERROR CONDITION,I2,5X,4HX = ,1PE10.3,5H  N =,I3,2X,1A4,
     17H(X,N) = ,E10.3,20H - EXECUTION DELETED)
      CALL EXIT
   15 PRINT 12,WORD(2),IER,R,N,WORD(2),BYA
      CALL EXIT
      END
```

```
      SUBROUTINE EXPAND
C     ------------------------------------------------------------------
C     THIS SUBROUTINE EXPANDS THE DATA OF GPHI(121) TO GPXI(361)       |
C     BY A FIVE POINT INTERPOLATION METHOD.                            |
C     ------------------------------------------------------------------
      IMPLICIT COMPLEX(G)
      COMMON/GULK/GPHI(121),NI,NF/GXBK/GPXI(361),NXI,NXF
      A1= -7.0/243.0
      A2= 70.0/243.0
      A3=210.0/243.0
      A4=-35.0/243.0
      A5=  5.0/243.0
      B1=-10.0/243.0
      B2=160.0/243.0
      B3=120.0/243.0
      B4=-32.0/243.0
      B5=  5.0/243.0
      DO 01 I=1,121
   01 GPXI(3*I-2)=GPHI(I)
      DO 02 I=2,119
      GPXI(3*I-1)=B1*GPHI(I-1)+B2*GPHI( I )+B3*GPHI(I+1)+B4*GPHI(I+2)
     1+B5*GPHI(I+3)
   02 GPXI(3*I)   =A1*GPHI(I-1)+A2*GPHI( I )+A3*GPHI(I+1)+A4*GPHI(I+2)
     1+A5*GPHI(I+3)
      GPXI(2)     =B1*GPHI(120)+B2*GPHI(  1)+B3*GPHI(  2)+B4*GPHI(  3)
     1+B5*GPHI(  4)
      GPXI(3)     =A1*GPHI(120)+A2*GPHI(  1)+A3*GPHI(  2)+A4*GPHI(  3)
     1+A5*GPHI(  4)
      GPXI(356)   =B1*GPHI(118)+B2*GPHI(119)+B3*GPHI(120)+B4*GPHI(121)
     1+B5*GPHI(  2)
      GPXI(357)   =A1*GPHI(118)+A2*GPHI(119)+A3*GPHI(120)+A4*GPHI(121)
     1+A5*GPHI(  2)
      GPXI(359)   =B1*GPHI(119)+B2*GPHI(120)+B3*GPHI(121)+B4*GPHI(  2)
     1+B5*GPHI(  3)
      GPXI(360)   =A1*GPHI(119)+A2*GPHI(120)+A3*GPHI(121)+A4*GPHI(  2)
     1+A5*GPHI(  3)
      RETURN
      END
```

A) Continued.

```
      SUBROUTINE VARIA(MM,VALUE)
C     ------------------------------------------------------------------
C     THIS SUBROUTINE COMPUTES SINTEGRAL(NI,NF)|GPHI-SUM(-MA,+MA)A(N)*
C     EXP(J*N*PHI)|**2 AND IS A TEST OF THE FIT OF THE A(N) TO GPHI.
C     ------------------------------------------------------------------
      IMPLICIT COMPLEX(A,G,H)
      DOUBLE PRECISION DPXA,DPYA,DPH
      COMMON/GBLK/GPHI(121),NI,NF/ABLK/A(63)/DBLK/DPXA(361),DPYA(361),
     1DPH,SPH,NPTH
      MA=(MM+1)/2
      DO 01 K=1,121
   01 DPXA(K)=0.0
      DO 03 NPHI=NI,NF
      HK=(0.0,0.0)
      HT=FLOAT(NPH-180)*SPH
      DO 02 K=1,MM
      AK=FLOAT(K-MA)*HT
      HK=CMPLX(0.0,AK)
   02 HK=HK+A(K)*CEXP(HK)
   03 DPXA(NPHI)=(CABS(GPHI(NPHI)-HK))**2
      CALL DOSP(DPH,DPXA,DPYA,121)
      VALUE=ANGL(DPYA(NF))
      WRITE(6,04)
   04 FORMAT('1','TEST OF SUBROUTINE VARIA. VALUES OF DPXA AND DPYA.')
      DO 06 I=1,41
      I41=I+41
      I82=I+82
      WRITE(6,05)I,DPXA(I),DPYA(I),I41,DPXA(I41),DPYA(I41),I82,DPXA(I82)
     1,DPYA(I82)
   05 FORMAT(' ',3X,I3,2X,2F16.12,5X,I3,2X,2F16.12,5X,I3,2X,2F16.12)
   06 CONTINUE
      RETURN
      END


      SUBROUTINE RYTOUT
      IMPLICIT COMPLEX (G)
      COMMON/GBLK/GPHI(121),NI,NF
      DO 01 I=1,41
      I41=I+41
      I82=I+82
      WRITE(6,02)I,GPHI(I),I41,GPHI(I41),I82,GPHI(I82)
   02 FORMAT(' ',3X,I3,2X,2F10.6,17X,I3,2X,2F10.6,17X,I3,2X,2F10.6)
   01 CONTINUE
      RETURN
      END
```

APPENDIX A4.

Miscellaneous programming comments.

Sample data module for the azimuthal program:
Pattern function data for a 1.0λ radius cylinder (ka=6.28)
followed by these data cards:

```
31  1121 32  6.283185   0.0015    1.00 0.28 0.05 0.01 2.0   0.6   1.4
 0
```

produces the locus diagram of Section 5.c.

Sample data module for the radial program:
Pattern function data for a 0.5λ radius cylinder (ka=3.14)
followed by these data cards:

```
41  1121  C  6.283185   0.0       1.0
     0.25      10.0       300.0        24.0
     0.25      10.0       330.0        24.0
T
 0
```

produces the scans of Section 5.e for a Fourier coefficient order of 20.

When the statements between 02 and 03 in the azimuthal program are replaced by:

```
      NTH=MOD(NTH+180,360)
      CALL TRANSG(NTH,XK,XR0)
```

the program can test double translations as described in Section 5.c.

A4 Continued.

The following subsections inserted one at a time between statement 08 and the DO 10 statement of the azimuthal program produce the alterations of Section 5.a. They require subroutine RYTOUT.

```
      WRITE(6,231)
  231 FORMAT('0','TRUNCATION OF GPHI TO 4 DECIMAL PLACES.')
      DO 331 I=1,121
      SAX=REAL(GPHI(I))*10000.0
      SBX=AIMAG(GPHI(I))*10000.0
      NA=INT(SAX)
      NB=INT(SBX)
      SAX=FLOAT(NA)*0.0001
      SBX=FLOAT(NB)*0.0001
  331 GPHI(I)=CMPLX(SAX,SBX)
      WRITE(6,431)
  431 FORMAT('1','TRUNCATED GPHI.')
      CALL RYTOUT
```

```
      WRITE(6,232)
  232 FORMAT('0','TRUNCATION OF GPHI TO 2 DECIMAL PLACES.')
      DO 332 I=1,121
      SAX=REAL(GPHI(I))*100.0
      SBX=AIMAG(GPHI(I))*100.0
      NA=INT(SAX)
      NB=INT(SBX)
      SAX=FLOAT(NA)*0.01
      SBX=FLOAT(NB)*0.01
  332 GPHI(I)=CMPLX(SAX,SBX)
      WRITE(6,432)
  432 FORMAT('1','TRUNCATED GPHI')
      CALL RYTOUT
```

```
      WRITE(6,233)
  233 FORMAT('0','ROUND OFF OF GPHI TO 4 DECIMAL PLACES.')
      DO 333 I=1,121
      GPHI(I)=GPHI(I)+(0.00005,0.00005)
      SAX=REAL(GPHI(I))*10000.0
      SBX=AIMAG(GPHI(I))*10000.0
      NA=INT(SAX)
      NB=INT(SBX)
      SAX=FLOAT(NA)*0.0001
      SBX=FLOAT(NB)*0.0001
  333 GPHI(I)=CMPLX(SAX,SBX)
      WRITE(6,433)
  433 FORMAT('1','ROUNDED GPHI.')
      CALL RYTOUT
```

```
      WRITE(6,234)
  234 FORMAT('0','ROUND OFF OF GPHI TO 2 DECIMAL PLACES.')
      DO 334 I=1,121
      GPHI(I)=GPHI(I)+(0.005,0.005)
      SAX=REAL(GPHI(I))*100.0
      SBX=AIMAG(GPHI(I))*100.0
      NA=INT(SAX)
      NB=INT(SBX)
      SAX=FLOAT(NA)*0.01
      SBX=FLOAT(NB)*0.01
  334 GPHI(I)=CMPLX(SAX,SBX)
      WRITE(6,434)
  434 FORMAT('1','ROUNDED GPHI')
      CALL RYTOUT
```

```
      WRITE(6,235)
  235 FORMAT('0','NOISE OF SIGMA=.05   ADDED.')
      IX=9979
      S=0.05
      SAM=0.0
      DO 335 I=1,121
      SAX=REAL (GPHI(I))
      SBX=AIMAG(GPHI(I))
      CALL GAUSS(IX,S,SAM,V1)
      IY=IX
      CALL GAUSS(IY,S,SAM,V2)
      IX=IY
      SAX=SAX+V1
      SBX=SBX+V2
  335 GPHI(I)=CMPLX(SAX,SBX)
      WRITE(6,435)
  435 FORMAT('1','NOISY GPHI.')
      CALL RYTOUT
```

```
      WRITE(6,236)
  236 FORMAT('0','NOISE OF SIGMA=.005  ADDED.')
      IX=36521
      S=0.005
      SAM=0.0
      DO 336 I=1,121
      SAX=REAL (GPHI(I))
      SBX=AIMAG(GPHI(I))
      CALL GAUSS(IX,S,SAM,V1)
      IY=IX
      CALL GAUSS(IY,S,SAM,V2)
      IX=IY
      SAX=SAX+V1
      SBX=SBX+V2
  336 GPHI(I)=CMPLX(SAX,SBX)
      WRITE(6,436)
  436 FORMAT('1','NOISY GPHI.')
      CALL RYTOUT
```

```
      WRITE(6,237)
  237 FORMAT('0','NOISE OF SIGMA=.0005 ADDED.')
      IX=1117
      S=0.0005
      SAM=0.0
      DO 337 I=1,121
      SAX=REAL (GPHI(I))
      SBX=AIMAG(GPHI(I))
      CALL GAUSS(IX,S,SAM,V1)
      IY=IX
      CALL GAUSS(IY,S,SAM,V2)
      IX=IY
      SAX=SAX+V1
      SBX=SBX+V2
  337 GPHI(I)=CMPLX(SAX,SBX)
      WRITE(6,437)
  437 FORMAT('1','NOISY GPHI.')
      CALL RYTOUT
```

REFERENCES

Boerner,W.M., Vandenberghe,F.H. and Hamid,M.A.K. (1971)
Can.J.Phys. 49, #7, 804.

Faddeyev,L.J. and Seckler,B. (1963)
Math.Phys. 4, 72.

Gabor,D. (1946) J.Inst.Elect.Eng. 93, (III), 429.

Gabor,D. (1961) Progress in Optics I. Edited by E. Wolf. (North-Holland, Amsterdam (1961))

Harrington,R.F. (1961) Time Harmonic Electromagnetic Fields. (McGraw-Hill, New York (1961))

Hildebrand,F.B. (1962) Advanced Calculus for Applications. (Prentice-Hall, Englewood Cliffs, N.J. (1962))

Howarth,B.A. (1970) Computer Subroutine HANK. Private Communication. (McGill University, Montreal, Canada)

Howarth,B.A. (1971) Scattered Field Map. Private Communication. (McGill University, Montreal, Canada)

Imbriale,W.A. and Mittra,R. (1970)
I.E.E.E. Trans.Ant.&Prop. AP 18, #5, 633.

Kerker,M. (1969) The Scattering of Light and other Electromagnetic Radiation. (Academic Press, N.Y.)

MacKay,D.M. (1950) Phil.Mag. 41, 289.

Mittra,R. (1970) Inverse Scattering and Remote Probing. Symposium on Computer Techniques for Electromagnetics and Antennas, U. of Illinois, Urbana, Illinois (September, 1970).

Shannon,C.E. (1948) Bell.Syst.Tech.J. 27, 379-423; 623-656.

Shannon,C.E. (1949) Proc.I.R.E. 37, 10.

Weiss,M.R. (1968) J.Opt.Soc.Am. 58, #17, 1524.

Weston,V.H. and Boerner,W.M. (1969)
Can.J.Phys. 47, #11, 1177.

Winthrop,J.T. (1971) J.Opt.Soc.Am. 61, #1, 15.